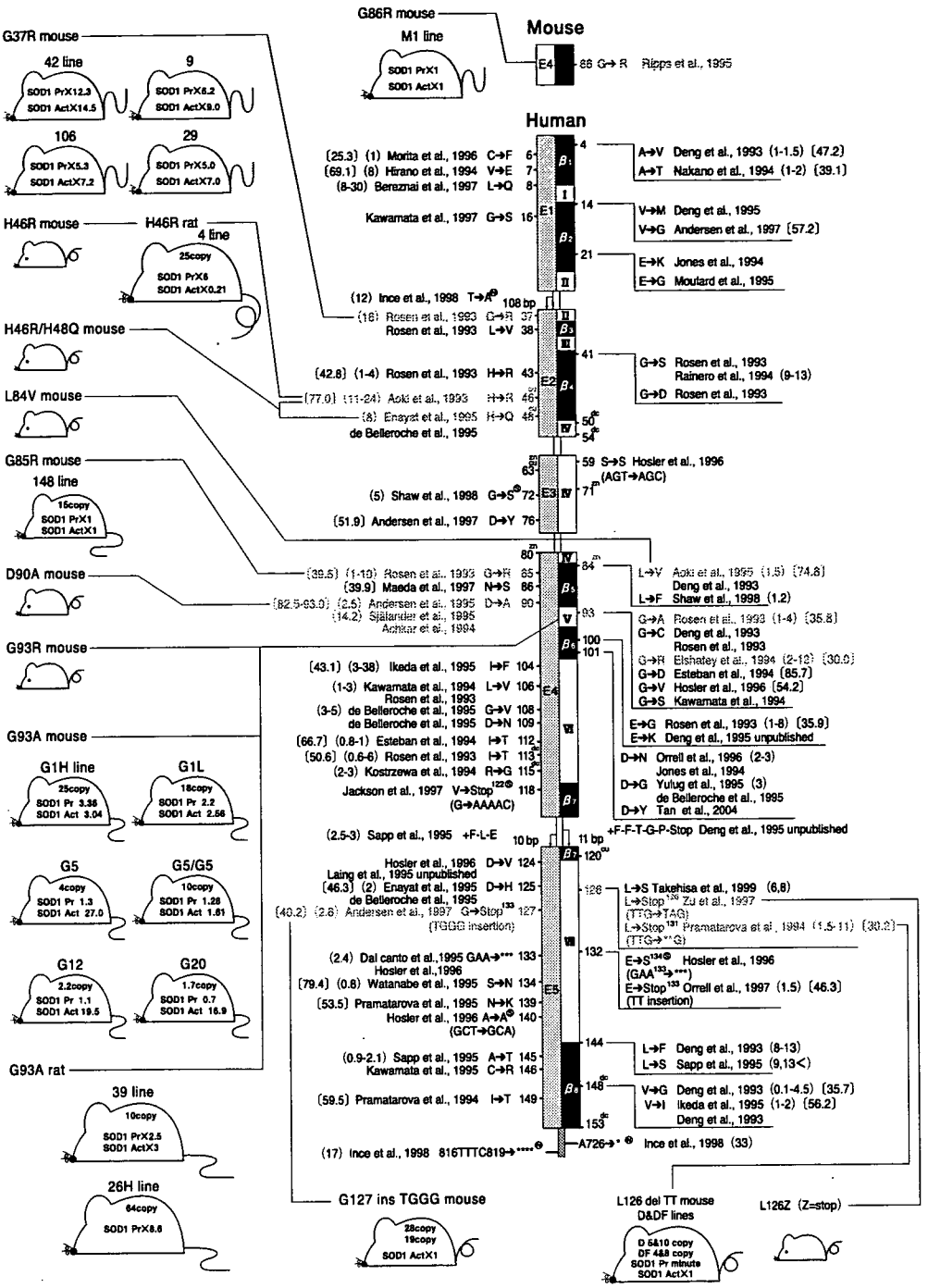

Fig. 2 Schema showing relationship between the main characteristics of transgenic rodents with mutant SOD1 and the main mutation of the human SOD1 gene. The main characteristics of transgenic rodents and human SOD1 gene structure are shown diagrammatically. With respect to transgenic rodents, the main characteristics of copy number, SOD1 protein level (SOD1 Pr), and SOD1 activity (SOD1 Act) in the G93A mouse (lines = G1H, G1L, G5, G5/G5, G12, G20), G37R mouse (lines = 42, 9, 106, 29), G85R mouse (line = 148), G86R mouse (line = M1), L126delTT mouse (lines = D, DF), G127insTGGG mouse, H46R rat (line = 4), and G93A rat (lines = 39, 26H) are shown within each rodent body; exact values for each unit are described in the text (See "Main characteristics of animal models based on SOD1"). As for the human SOD1 gene structure, *large blue areas* (E1–E5) = exon 1 to 5; *small open areas* = intron; *small dark gray area* = 3 prime untranslated region. *Large black areas* (beta-sheets) = beta-sheet 1–8; *large open areas* (beta-loops) = beta-loops I to VII [IV, VII = active site; III, VI = Greek key]. Superscript Cu = copper binding site; superscript Zn = zinc binding site; superscript dc = dimer contact. Amino acid or nucleotide substitutions are indicated at appropriate codons according to the accepted international nomenclature. Even SALS has an SOD1 abnormality; each encircled superscript S indicates the SALS. Each encircled superscript N indicates ALS without a familial history. Disease durations (years) are shown in parentheses. FALS shows various disease durations according to the type of SOD1 gene mutation responsible; enzyme activities (% value relative to normal control erythrocytes) are shown in *brackets*. Mouse SOD1 gene structure of exon 4 (E4) is shown in *yellow*

are summarized in this paragraph in detail and shown schematically in Fig. 2. There are six major strains of ALS transgenic rodents carrying human mutant SOD1: G93A mice (lines: G1, G5, G12 and G20) [19–21, 36], G37R mice (lines: 42, 9, 106 and 29) [98], G85R mice (lines: 221, 164, 103, 148, 74, 46, 87 and 124) [10], H46R/H48Q mice (lines:139, 73, 67, and 58) [96], H46R rats (line: 4) [2, 72], and G93A rats (lines: 39) [2, 72] and 26H [43]). In addition, seven types of transgenic mice bearing human mutant SOD1 have been produced: G93R mice [31], D90A mice [49], H46R mice [1], L84V mice [1], L126delTT mice [97], L126Z (Z = stop) mice [23], and G127insTGGG mice [48]. There is a major line of transgenic mice carrying mouse G86R SOD1 (lines: M1, M2 and M3) [81].

With respect to G93A mice [19–21, 36], the original mouse strain G1-G93A carries 18.0 ± 2.6 transgene copy numbers expressing 4.1 ± 0.54 ng human SOD1 protein per μg of total protein (ng human SOD1) with SOD1 activity of 42.6 ± 2.1 U per μg of total protein (U). G5-G93A mice with 4.0 ± 0.6 copies show 1.3 ± 0.21 ng human SOD1 with 27.0 ± 2.9 U SOD1 activity. G12-G93A mice with 2.2 ± 0.8 copies exhibit 1.1 ± 0.22 ng human SOD1 with 19.5 ± 0.8 U SOD1 activity, and G20-G93A mice with 1.7 ± 0.6 copies express 0.7 ± 0.06 ng human SOD1 with 16.9 ± 0.4 U SOD1 activity. The original G1 line differentiates into two sub-lines derived from the same founder. These two sub-lines, named G1H and G1L, express different transgene copy numbers: G1H-G93A mice carrying 25 transgene copy numbers express 3.36 ± 0.84 ng SOD1 protein per μg soluble brain protein (ng SOD/sbp) with SOD1 activity of 3.04 ± 0.71 U per μg sbp (U/sbp), and G1L-G93A mice expressing 18 copies show 2.20 ± 0.9 ng SOD1/sbp with 2.56 ± 0.23 U/sbp SOD1 activity. G5/G5-G93A mice have been newly generated from G5-G93A mice: G5/G5-G93A mice with 10 copies express 1.28 ± 0.44 ng SOD1/sbp with 1.61 ± 0.14 U/sbp SOD1 activity.

With respect to G37R mice [98], the spinal cord tissues of G37R-42 mice express the human SOD1 protein at a level 12.3 times that of the endogenous mouse SOD1 protein with SOD1 activity 14.5 times higher than the control, G37R-9 mice show a 6.2-fold SOD1 protein level in spinal cord tissues and 9.0-fold SOD1 activity relative to the control, G37R-106 mice show a 5.3-fold SOD1 protein level and 7.2-fold SOD1 activity, and G37R-29 mice express a 5.0-fold SOD1 protein level and 7.0-fold SOD1 activity. There is no detailed description of transgene copy numbers in the original literature.

With regard to G85R mice [10], eight lines have been established with transgene copy numbers of 2–15, and lines 221, 164, 103, 148, 74, 87, 124 show a clinical phenotype. The SOD1 protein level (human/mouse) in these lines is 0.5, 0.8, 0.6, 1.0, 0.2, 0.6 and 0.6, respectively. Among seven lines in G85R mice, G85R-148 mice carrying 15 transgene copies numbers express the same SOD1 activity comparable to the control.

As for G86R mice [81], although there were three original lines of M1, M2 and M3 in G86R mice, only line M3 has not been perpetuated. M1 and M3 show a clinical phenotype, whereas all M2 mice appear phenotypically normal. The M1 line exhibits an equal amount of total SOD1 protein to the control and show almost identical SOD1 activity. Since G86R mice express murine mutant G86R SOD1, they are advantageous for researchers in that the mouse genomic sequence can be used to reproduce the mutation in SOD1.

With regard to transgenic rats with human mutant SOD1, H46R-4 rats carrying 25 transgene copy numbers express human SOD1 protein at 6 times the level of endogenous rat SOD1 and show SOD1 activity in the spinal cord tissues that is 0.21 times the control activity [2, 72]. G93A-39 rats expressing 10 transgene copies express 2.5 times the human SOD1 protein level and show SOD1 activity in spinal cord tissues that is 3 times the control activity [2, 72]. G93A-26H rats with 64 copies express 8.6 times the human SOD1 protein level, and their founder rats (G93A-26HL) with 72 copies show 10.4 times the human SOD1 level [43].

Neurology and neuropathology of animal models based on SOD1

The first report of transgenic mice expressing human mutant SOD1 was published by Gurney et al. [36]. Therefore, these mice—known as Gurney mice—are the most well known and have been used extensively by many researchers. Among these Gurney mice, the G1H- and G1L-G93A strains are the most widely studied [20, 36]. The first clinical symptom of G1H-G93A mice is reportedly a fine tremor in one or more limbs, which appears at approximately 90 to 100 days of age [20]. On the basis of the author's experimental experience with G1H- and G1L-G93A mice, the term "jittering" seems to be a more appropriate descriptor for the early clinical symptoms they show, rather than "tremor". Although spontaneous jittering/tremor as a single sign is not specific as the initial symptom, it is frequently observed in one or both hind legs when motor work loading such as the extension reflex is applied at a very early clinical stage. Many G1H-G93A mice at approximately 100 days of age exhibit clinical symptoms such as slow walking without agility due to muscle weakness, limp tail, jittering/tremor sometimes associated with motor work loading, and incomplete paresis of a single hind limb. These clinical symptoms can be regarded as significant signs of limb paresis and/or muscle weakness. From the author's experience [52, 59], clinical onset in almost all

G1H-G93A mice (B6SJL-TgN[SOD1-G93A]1Gur, JR2726) originating from Jackson Laboratory (Bar Harbor, ME, USA) occurs at about 100 days after birth, and death occurs at approximately 120 days. Neurologically, almost all G1H-G93A mice show a uniform clinical course, beginning with muscle weakness and/or paresis in the hind limbs, followed by ascent of paresis or paralysis to the forelimbs, until by the end stage the mice show severe quadriplegia, lying sideways or in a moribund state.

The essential cytopathological features of transgenic rodents overexpressing human mutant SOD1 are motor neuron loss with astrocytosis, the presence of SOD1-positive inclusions including LBHIs/Ast-HIs, and vacuole formation. Among these three major pathologic features, motor neuron loss with gliosis is the most essential, and is shared between human ALS and human mutant SOD1 transgenic rodents. In the G1H-G93A spinal cord [52, 59], the number of anterior horn cells at 90 days of age is not decreased significantly in comparison with age-matched littermates, whereas neuropil and/or neuronal intracytoplasmic vacuolation is already evident (Fig. 3a). The numbers of anterior horn cells in G1H-G93A mice at 100 days of age are slightly decreased, with abundant vacuoles and few inclusions (Fig. 3b). At 110 days, the mice demonstrate loss of anterior horn cells, some inclusions and vacuole formation. At 120 days, the mice exhibit quadriplegia and/or a moribund state, with severe loss of anterior horn cells and prominent inclusion pathology, although vacuolation pathology is less marked than that at disease onset (Fig. 3c). Although the author has utilized over 200 G1H-G93A mice hitherto and observed that the numbers of anterior horn cells in G1H-G93A mice at 100 days are slightly decreased, a review paper from Bendotti and Carri has indicated that there is 44% loss of motor neurons at 105 days [8]. This difference might be based on variations in the methods used to perpetuate the original G1H-G93A mice among researchers' institutions, the presence or absence of backcross breeding of B6 mice × original G1H-G93A mice, and differences in quantitation methodologies among researchers. Therefore, researchers need to be sufficiently aware of the differences in the genetic background of G1H-G93A mice and research methodologies before drawing conclusions. Clinical onset in most G1L-G93A mice (B6SJL-TgN[SOD1-G93A]1 Gur^{dl}, JR2300) from Jackson Laboratory occurs at about 185 days after birth, and death occurs after 250 days. G1L-G93A mice examined at 90, 100, 120, and 150 days of age show only vacuolation pathology without significant neuronal loss or inclusion pathology, whereas those aged 180 days reveal slightly decreased numbers of neurons with many vacuoles and a few inclusions. At the terminal stage after 250 days of age, there is significant loss of anterior horn cells, with both inclusion and vacuolation pathologies [52, 59].

Among transgenic rats with human mutant SOD1 [2, 52, 59, 72], H46R line-4 rats develop motor deficits at approximately 145 days of age, whereas G93A line-39 rats show clinical signs at around 125 days. The number of anterior horn cells in H46R rats at 110 days is not significantly decreased in comparison with age-matched littermates. The anterior horn cells of H46R rats at 135 days are slightly decreased in numbers and show inclusions, whereas at 160, 170 and over 180 days, the anterior horn cells are markedly decreased, and show severe inclusion pathology, featuring neuronal LBHIs and Ast-HIs. With respect to G93A rats, the number of anterior horn cells at 70, 90 and 110 days of age is almost the same as that in age-matched littermates, although at 90 and 110 days of age there is marked vacuolation pathology. At 130, 150 and over 180 days of age, there is marked loss of anterior horn cells, along with both inclusion and vacuolation pathology.

Invariably, the core pathology of rodents carrying mutant SOD1 is the lower motor neuron degeneration/death. As far as can be clarified from the original literature, however, the pathological lesions of G93A mice [19–21, 36] are distributed mainly in the spinal cord anterior horn, brainstem motor nuclei, brainstem reticular formation, dorsal motor nucleus of the vagus nerve, red nucleus, interpeduncular nucleus, and substantia nigra. In G37R mice [98], the areas of degeneration are mainly the spinal cord anterior horn, brainstem motor nuclei, and ventral and lateral white matter of the spinal cord. Vacuole formation is also evident in the olfactory bulb, pyriform cortex, striatum, thalamus, hypothalamus, and choroid plexus. G85R mice show severe neuronal abnormalities in the spinal cord ventral motor neurons, including small neurons near the central canal, and rare interneurons of the dorsal horns, as well as brainstem neurons, especially in the pons [10]. G86R mice show a pronounced motor neuron loss within the spinal cord ventral horns [81]. In the brainstem motor neurons, G86R mice show severe motor neuron depletion in the facial nuclei, while the oculomotor and hypoglossal nuclei show less extreme involvement [75]. From a neurochemical viewpoint, G86R mice exhibit vulnerability of the spinal cord motor neurons, which are positive for pNFP, CAT and calretinin proteins [68]. In H46R-4 and G93A-39 rats [2, 72], the central nervous system lesions are located in the spinal cord ventral horns and brainstem motor nuclei, but no pathology is evident in the cerebral cortex and cerebellum. G93A-26H rats are pathologically similar to G93A-39 rats, showing motor neuron loss with prominent vacuolation [43].

Since the pathology of ALS rodents bearing mutant SOD1 is expressed primarily as lower motor neuron degeneration/death, the number of reports describing upper motor neuron pathology in these models is limited in comparison

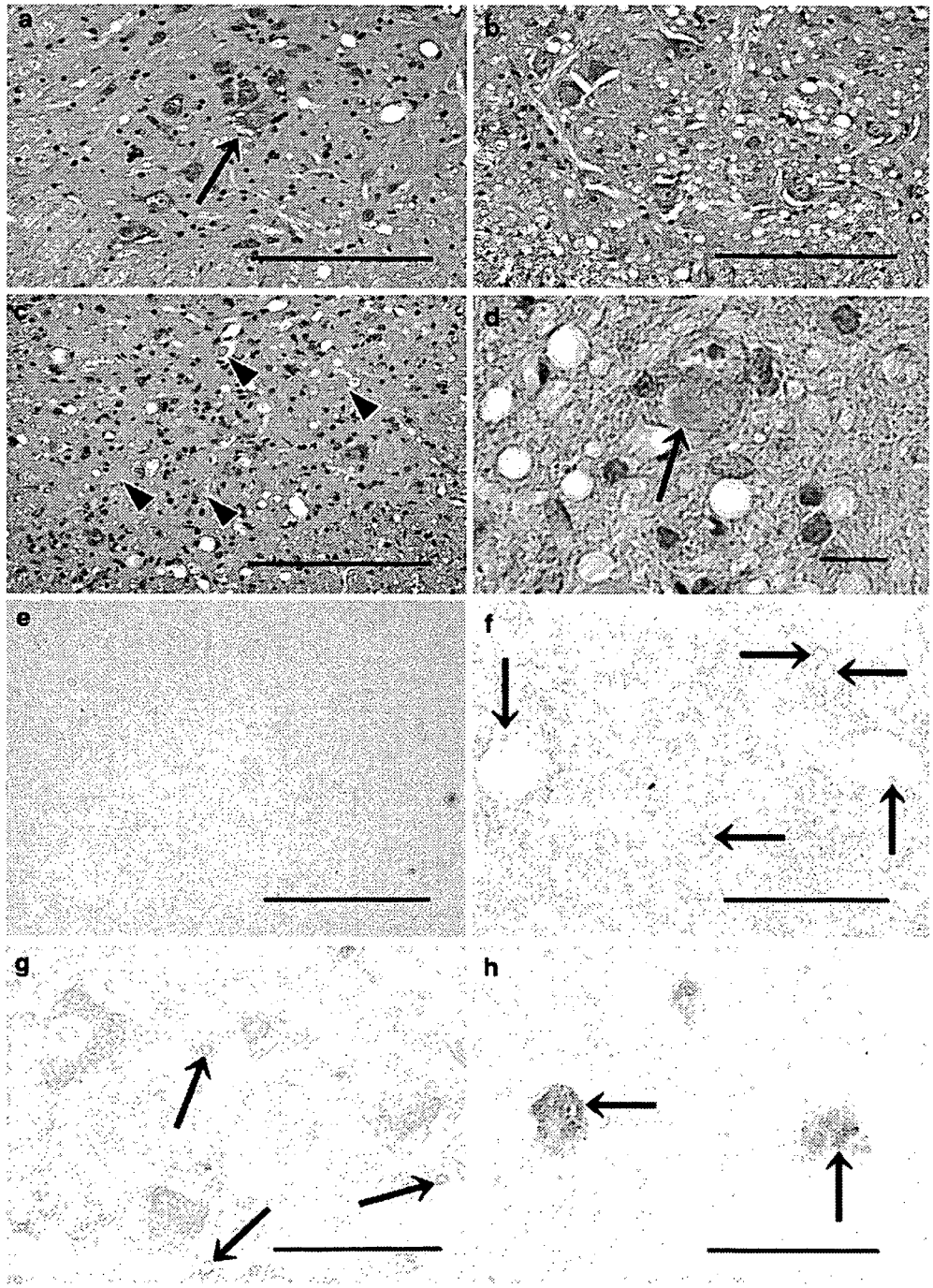

Fig. 3 Neuropathological findings of G1H-G93A mice as a gold-standard ALS model. **a** The number of anterior horn cells at 90 days of age is not decreased significantly; approximately 10 anterior horn cells can are observed, although an anterior horn cell with intracytoplasmic vacuolation is evident (*arrow*). **b** The numbers of anterior horn cells at 100 days of age are slightly decreased; about eight anterior horn cells can be seen, whereas abundant vacuoles are observed. **c** At 120 days, when the mouse is quadriplegic and moribund, there is severe loss of anterior horn cells and prominent inclusion pathology (*arrowheads*), although the vacuolation pathology is less marked than that at disease onset (in Fig. **b**). There is an inverse correlation between the number of vacuoles and the number of inclusions. **a–c** H&E. Scale bar **a** (also for **b, c**) 200 μm. **d** Light micrograph of a round neuronal LBHI (*arrow*) in a spinal anterior horn cell of a G1H-G93A mouse. This LBHI is observed in the cytoplasm of an anterior horn cell, and is composed of eosinophilic core with paler peripheral halo. Vacuolation pathology is evident in the neuropil. H&E. Scale bar **d** 20 μm. **e-h** Immunostaining with antibody against human SOD1 in the spinal cord anterior horn of the G1H-G93A mouse. This antibody (MBL, Nagoya, Japan) recognizes only human SOD1, i.e., mutant human G93A-SOD1. **e** Littermate mouse, showing no expression of G93A-SOD1. **f** In a 90-day-old G1H-G93A mouse, G93A-SOD1 is expressed mainly in the neuropil, and sometimes expressed intensely within the rims of vacuoles in the neuropil and motor neuron cytoplasm (*arrows*). However, it is not expressed in the motor neurons. **g** In a 110-day-old G1H-G93A mouse, G93A-SOD1 is expressed within the motor neuron cytoplasm in addition to the vacuole rims in the neuropil (*arrows*). **h**: In a 120-day-old G1H-G93A mouse, LBHIs are strongly positive for G93A-SOD1 (*arrows*). Scale bar **e** (also for **f–h**) 10 μm

with more frequent focusing on lower motor neuron pathology. This can be explained mainly in terms of the anatomical difference in the corticospinal tract system between humans and rodents: the main corticospinal tracts in the human spinal cord are the lateral and anterior columns, while the main spinal cord pyramidal tracts in rodents are the dorsal columns. Another major consideration is that even at necropsy with end-stage pathology, SOD1-mutated FALS, which is the prototype for these models, demonstrates only slight or mild corticospinal tract degeneration. Although there are a relatively few reports, some are pertinent. One group has reported that 110-day-old G1H-G93A mice demonstrate degeneration of the corticospinal and bulbospinal systems, in which 53% of corticospinal, 41% of bulbospinal and 43% of rubospinal neurons are lost (the bulbospinal neuron system in mice comprises three systems: rubospinal, vestibulospinal and reticulospinal neurons) [103]. Another group has reported that G85R mice at the end stage show progressive axonal degeneration of corticospinal tracts in the dorsal and lateral columns of the spinal cord [101].

Inclusion pathology

Ever since Hirano et al. [42] emphasized the presence of neuronal LBHIs in the anterior horn cells of FALS patients with posterior column involvement in 1967, and the author discovered Ast-HIs in 1996 [53], LBHI/Ast-HI have been considered pathognomonic features of mutant SOD1-linked FALS with posterior column involvement, which is the prototype form of human mutant SOD1 transgenic rodents, and in these transgenic rodents neuronal LBHIs are frequently observed in the soma (Fig. 3d) and neurites, although rarely in axons. Although Ast-HIs are sometimes found in only long-surviving patients with SOD1-mutated FALS [53, 54], they are frequently seen in G85R mice and H46R rats as well as in both G1H-/G1L-G93A mice and G93A rats at terminal stage [56, 59].

The author has examined six different lines of G1H-/G1L-G93A mice, G85R-148 mice, L84V mice, and H46R-4 and G93A-39 rats by electron microscopy, and all show almost identical ultrastructural features of neuronal LBHIs and Ast-HIs. Interestingly, neuronal LBHIs observed in both SOD1-mutated rodents and humans have a similar ultrastructure, being composed mainly of randomly oriented granule-coated fibrils approximately15–25 nm in diameter and granular materials. Ast-HIs seen in both SOD1-mutated rodents and humans also have the same ultrastructure. Therefore, the essential ultrastructural common components of neuronal LBHIs and Ast-HIs in SOD1-mutated rodents and humans are granule-coated fibrils about 15–25 nm in diameter and granular materials. As the inclusions develop, the granule-coated fibrillar component increases and the amount of granular material decreases, suggesting that the former might be derived from the latter [57].

It is of considerable interest that LBHIs/Ast-HIs observed in SOD1-mutated rodents are light- and electron-microscopically identical to those in patients with SOD1-mutated FALS. The presence of LBHI/Ast-HI is a morphological hallmark of cells affected by mutant SOD1 [58], and the formation of LBHI/Ast-HI is reported to be correlated with disease severity and progression [90]. However, the mechanism by which SOD1 mutation in vivo leads to the formation of 15–25-nm granule-coated fibrils as an essential component of LBHI/Ast-HI remains poorly defined. An important clue for explaining the formation of the granule-coated fibrils as an ultrastructural hallmark of mutant SOD1 has been reported: the same granule-coated fibrils as those in SOD1-mutated cells in vivo are induced by endoplasmic reticulum (ER) stress in vitro using neuroblastoma cells overexpressing human mutant L84V SOD1 [100]. Transgenic mice with L84V SOD1 show aberrant aggregation of the ER in association with early-stage neuronal LBHIs, suggesting that the LBHIs might arise as a result of ER dysfunction [100]. Collectively, the presence of LBHI/Ast-HI is a light-microscopical hallmark of SOD1-mutated cells, and the 15–25-nm granule-coated fibrils as an essential component of the LBHI/Ast-HI provide ultrastructural authentication of SOD1-mutated cells. In marked contrast, Bunina bodies are not found in the transgenic rodents bearing mutant SOD1.

Vacuolation pathology

With regard to vacuolation pathology, although transgenic rodents expressing mutant SOD1 exhibit vacuoles of various sizes in neurons and neuropil, similar features are not evident in autopsy cases of mutant SOD1-related FALS, which is the prototype of the mutant SOD1 transgenic rodent. This vacuolation pathology is also undetectable in mutant SOD1-unrelated FALS and SALS. Ultrastructurally, the vacuolation is evident in somata, dendrites and axons of motor neurons. At an early stage, these alterations occur in the rough ER and mitochondria. In particular, perinuclear vacuoles in somata at the early stage are derived from dilated ER cisternae. As the disease progresses, the number of mitochondria-derived vacuoles increases, while the number of vacuoles originating from the ER decreases. Mitochondria-derived vacuoles originate through expansion of the mitochondrial intermembrane space and extension of the outer mitochondrial membrane [40]. These vacuoles are apparently more abundant at disease onset, and decline thereafter; vacuole formation itself is reported to be related to disease onset rather than disease progression [61]. There are abundant vacuoles and few LBHIs in the early course of degeneration in G1L-G93A and G1H-

G93A mice (Fig. 3b), and mice at the terminal stage show less abundant vacuoles and many LBHIs (Fig. 3c), i.e., there is a significant inverse correlation between the numbers of vacuoles and LBHIs [91]. Another important finding in G1H- and G1L-G93A mice at the presymptomatic stage is fragmentation of the Golgi apparatus in the spinal cord anterior horn cells [69].

Contribution of mutant SOD1 in each cell type

Transgenic rodents overexpress human mutant G93A SOD1 in all cells because the transgene is driven by a non-cell-specific endogenous promoter. On the other hand, there are transgenic mice in which mutant SOD1 expression is driven by a neuron-specific promoter such as the neurofilament light chain. In transgenic mice whose anterior horn cells specifically overexpress mutant SOD1, neither motor neuron impairment nor degeneration is evident [80]. Transgenic mice that overexpress the mutant SOD1 transgene in neurons after birth also do not show motor neuron pathology [65]. Some other types of transgenic mice overexpress mutant G86R SOD1 only in astrocytes under control of the GFAP promoter. Despite the fact that these mice develop astrocytosis, they show no motor neuron degeneration and develop normally [34]. Although neurons or astrocytes play very important role in ALS pathogenesis, it is of considerable interest that mutant SOD1, when over expressed either in neurons or astrocytes, does not sufficiently contribute to the onset of ALS. In culture study, conversely, astrocytes expressing mutated SOD1 kill spinal primary and embryonic mouse stem cell-derived motor neurons [73]. In addition to neurons and astrocytes, microglia are closely related to neuron injury not only in ALS but also other neurodegenerative disorders. Approaches such as the use of a deletable mutant SOD1 transgene have demonstrated that diminishing mutant SOD1 within microglia has little effect on the early disease phase but sharply slows later disease progression: i.e., SOD1 mutated motor neurons are a determinant of onset and early disease, and mutant accumulation within microglia accelerates disease progression [9]. Interestingly, microglia themselves have a double-edged sword effect; wild-type microglia can extend the survival of G93A mice with PU.1 knockout mice (which are unable to develop myeloid and lymphoid cells) by using bone marrow transplantation [6]. Since retraction of motor axons from synaptic connections to muscle is among the earlier presymptomatic morphological findings in SOD1-mutated mice, muscle itself is also a likely primary source of mutant SOD1 toxicity. However, use of a deletable mutant gene to eliminate mutant SOD1 from muscle does not affect disease onset or survival: SOD1-mutant-mediated damage within muscles is not a significant contributor to non-cell-autonomous pathogenesis in ALS [66].

Relation between mutant SOD1 and disease progression

Unlike patients with SOD1-mutated FALS, transgenic rodents bear both human mutant SOD1 and native endogenous rodent SOD1. Native endogenous rodent SOD1 catalyzes the conversion of the superoxide radical to hydrogen peroxide and molecular oxygen. Even overinduced human mutant SOD1 also detoxifies the superoxide radical, which is a source of reactive oxygen species generated from aerobic organisms, and protects cells, including motor neurons, from oxidative injury. Based on the gain-of-function theory, human mutant SOD1 itself acts as a cytotoxic factor, and in G1H-G93A mice human mutant G93A-SOD1 shows cytotoxicity for motor neurons. In 90-day-old G1H-G93A mice that show no significant motor neuron loss and only slight vacuolation pathology, G93A-SOD1 is already present but its expression level is not marked, and immunohistochemically it is expressed mainly in the neuropil, sometimes being expressed intensely within the rims of vacuoles in the neuropil and motor neuron cytoplasm (Fig. 3e,f). In contrast, motor neurons do not express mutant SOD1 (Fig. 3e,f). In 100-day-old G1H-G93A mice that demonstrate a slightly decreased number of motor neurons and prominent vacuolation pathology, mutant G93A-SOD1 is highly expressed in comparison with the level at 90 days of age. At 110 days, the mice that show loss of anterior horn cells with some inclusions and vacuole formation also exhibit high expression of mutant G93A-SOD1, which morphologically is located within the motor neuron cytoplasm and the vacuole rims in the neuropil (Fig. 3e,g). End-stage G1H-G93A mice that show severe motor neuron loss as well as vacuolation and inclusion pathologies demonstrate high expression of mutant G93A-SOD1, and immunohistochemically mutant G93A-SOD1 is aggregated and sequestered into the LBHIs, which are strongly positive for mutant G93A-SOD1 (Fig. 3e, h). Considered in connection with the abundance of neuropil vacuoles and few LBHIs at the early stage, and the fact that mice at the terminal stage show many LBHIs and less abundant vacuoles, as well as the accumulation of mutant G93A-SOD1 in vacuoles at the early stage and marked aggregation of mutant G93A-SOD1 in LBHIs at the late stage, it is possible that cytotoxic mutant G93A-SOD1 within vacuoles at the early stage leaks into the neurons and then aggregates within neurons as LBHIs with disease progression. Along with disease progression, there is a breakdown of cytotoxic mutant SOD1 sequestration in vacuoles, and the mutant SOD1 aggregates in motor neurons, resulting in their degeneration/death.

Development of rats with human mutant SOD1

The ultimate aim of developing transgenic rodents expressing human mutant SOD1 are as follows: to gain an

understanding of the mechanism of motor neuron death in the presence of mutant SOD1, and to test new ALS therapies. Freshly obtained mouse spinal cord including the nerve roots, cauda equina and filum terminale, weighs only about 110 mg and is approximately 4 cm in length. In order to perform more extensive analysis of the mechanism of motor neuron death and to devise new ALS therapies that are difficult or impossible to explore using the small spinal cord of the mouse, transgenic rats expressing human mutant SOD1 have been developed [2, 43, 72]. As rats are a larger species than mice, they are easier to use in studies involving manipulations of spinal fluid (e.g., implantation of intrathecal catheters for chronic therapeutic studies and CSF sampling) and the spinal cord (e.g., direct administration of viral and cell-mediated therapies).

Relationship between ALS and TDP-43

The 43-kDa TAR DNA-binding protein (TDP-43) is localized to the nucleus. Originally, TDP-43 was identified as a component of ubiquitinated inclusions in frontotemporal lobar degeneration with ubiquitinated inclusions (FTLD-U) and ALS [3, 74]. Analyses of TDP-43 immunohistochemistry in SALS (two patients), mutant SOD1-unrelated FALS (two patients) and ALSD (one patient) have shown TDP-43-immunoreactive inclusions such as SLI/RHI in the anterior horn cells of the spinal cord [95]; as mentioned above, SLI/RHI are characteristic morphological structures in ALS, and mutant SOD1-unrelated FALS is neuropathologically indistinguishable from SALS. TDP-43 immunoreactivity has also been detected in the motor neurons of the hypoglossal nucleus in 4 patients with FTLD-MND/ALSD and 11 patients with ALS; TDP-43-positive structures include SLI/RHI [26]. Although Bunina bodies are a pathognomonic structure in SALS, mutant SOD1-unrelated FALS and FTLD-MND/ALSD, Bunina bodies themselves are negative for TDP-43 [95]. With regard to mutant SOD1-related motor neuron death, LBHIs, which are characteristic structures in mutant SOD1-related FALS with A4T (one patient) and D101Y (one patient) reportedly do not express TDP-43 [95]. In SALS (one patient) as well as mutant SOD1-related FALS with A4T (one patient) and I113T (one patient), TDP-43 is mislocalized from the nucleus to the cytoplasm [83]. Especially, one case of SALS was reported to show ubiquitin-positive RHIs with TDP-43 staining pattern [83]. By marked contrast, human mutant G93A, G37R and G85R SOD1-transgenic mice do not show any TDP-43 abnormalities including either TDP-43-positive inclusions or TDP-43 mislocalization [83]. It could be stated that in general, TDP-43 contributes to mutant SOD1-unlinked motor neuron degeneration, whereas mutant SOD1-linked motor neuron degeneration may not be essentially related to TDP-43 abnormality; in particular, human mutant SOD1 transgenic mice do not show TDP-43 abnormality [83].

Mouse models of ALS2

As already mentioned, SOD1 mutations have been identified as a cause of autosomal dominant FALS [22, 84]. Mutation in a second ALS-related (ALS2) gene has also been identified as the cause of a rare autosomal recessive form of juvenile-onset ALS, also referred to as ALS2 [7, 37, 102], as well as juvenile-onset primary lateral sclerosis (PLS) [37], and infantile-onset ascending hereditary spastic paralysis (HSP) [24, 29, 35]. In humans, the ALS2 gene is located on chromosome 2 at position 33.2, and encodes a protein called ALS2 protein or alsin. ALS2 protein is produced in a wide range of normal tissues, with the highest amounts in the brain and spinal cord. ALS2 protein is composed of 1,657 amino acids with three predicted guanine nucleotide exchange factor (GEF)-like domains [37, 102]: an N-terminal regulator of chromatin condensation (RCC 1)-like domain (RLD) homologous to GEF for Ran GTPase [77], middle Dbl homology (DH) and pleckstrin homology (PH) (DH/PH)-like domains resembling GEF for Rho GTPase [87], and a C-terminal vacuolar protein sorting 9 (VPS9)-like domain similar to GEF for Rab5 GTPase [79]. This ALS2 protein is particularly abundant in motor neurons. ALS2 protein is preferentially associated with the cytoplasmic face of the endosomal membrane [79]. Although the function of ALS2 protein in motor neurons is unclear, it may play an important role in regulating cell membrane organization and the movement of molecules within motor neurons. Therefore, it would be expected to play a role in the development of axons and dendrites. It is unclear how and why loss of ALS2 protein function causes the ALS2-linked diseases: ALS2, juvenile-onset PLS, and infantile-onset ascending HSP. In order to gain insight into the physiological role of ALS2 protein and the pathogenesis of ALS2-linked diseases, four types of ALS2 knockout mice have been successfully developed.

The ALS2 knockout mice with disruption of exon 3 of the murine ALS2 gene reported by Cai et al. [13] show a higher anxiety response as well as an age-dependent deficit of motor coordination and learning. Histopathologically and biologically, ALS2 knockout mice are characterized by a lack of neuropathological abnormality, no alteration of peripheral nerve conduction or electromyography features, susceptibility to oxidative stress, and increased susceptibility to glutamate receptor-mediated excitotoxicity. In the ALS2 knockout mice reported by Hadano et al. [38], exon 3 of the murine ALS2 gene is disrupted by inserting a stop codon. These mice demonstrate no obvious developmental,

reproductive or motor abnormalities. However, histopathologically and biologically, they are characterized by an age-dependent decrease in the size and number of ventral motor axons and cerebellar Purkinje cells, astrocytosis and microglial activation in the spinal cord and brain, motor unit remodeling and fiber redistribution in skeletal muscle, and slightly affected endosomal dynamics. ALS2 knockout mice with disruption of both exons 3 and 4 of the murine ALS2 gene reported by Devon et al. [25] show mild hypoactivity. Neuropathologically, at the age of 12 months, they show significantly smaller cortical motor neurons, and in addition, marked diminution of Rab5-dependent endosome fusion activity and disturbance in endosomal transport of the insulin-like growth factor 1 and BDNF receptors. ALS2 knockout mice with disruption of exon 4 of the murine ALS2 gene reported by Yamanaka et al. [101] demonstrate slowed movement without muscle weakness and progressive axonal degeneration in the lateral spinal cord. Significantly, all four of these ALS2 knockout murine models show no human ALS2-like symptoms and are not neurologically analogous to humans with ALS2.

Among previously reported human patients with ALS2-linked disease, the members of a Tunisian family with 138delA ALS2 gene mutation showed development of spasticity in all limbs between 3–10 years of age [7, 37, 102], and their clinical symptoms might be classifiable as part of a spectrum of HSP rather than typical ALS. The members of a Kuwaiti family with 1425_1426delAG ALS2 gene mutation showed infantile-onset spastic paralysis without lower motor neuron involvement at 1–2 years of age [37]. Members of a Saudi Arabian family with1867_1868delCT ALS2 gene mutation developed PLS between 1–2 years of age [33, 102]. Up to now, eight additional ALS2-linked diseases have been reported [24, 29, 30, 35, 62], and a major common characteristic is infantile-onset spastic paralysis, reflecting upper motor disturbance. Although lower motor neuron impairment has been reported in a limited number of patients with ALS2 gene mutation, the majority of ALS2 gene mutations appear to be linked to upper motor neuron diseases from the viewpoint of human clinical data of 11-type ALS2-linked diseases. Although to the author's knowledge there has been no reported autopsy case of ALS2, detailed neuropathological data from human ALS2 autopsy cases would clarify this point. In this context, although the author is unable to address the similarities and differences between human ALS2 and ALS2 animal models from a neuropathological viewpoint, it might be concluded that data from ALS2 knockout mice and ALS2-linked diseases mentioned above would become more valuable for clarifying the pathogenesis of human ALS2 if detailed human ALS2 autopsy data were also available.

Animal models based on cytoskeletal abnormalities

Animal models based on neurofilament abnormalities

The neuron cytoskeleton consists of three major filaments: actin microfilaments, microtubules, and neurofilaments. Neurofilaments biochemically comprise three different isoforms known as neurofilament triplet proteins: light subunit (68 kDa), medium subunit (160 kDa), and heavy subunit (200 kDa). Ultrastructurally, neurofilaments are approximately 10 nm in diameter, but in cross-section they appear tubular in structure with a narrow central electron-lucent core, and have fine side arms. Their size places them in the so-called "intermediate filaments" morphologically.

Neurofilament-lacking mice

Mice lacking any of the neurofilament triplet protein genes show no developmental problems [82]. However, mice lacking the neurofilament light subunit show a lack of intermediate filament structure, axonal hypotrophy, and aggregation of neurofilament medium and heavy subunit in motor neurons, although significant motor neuron loss is not evident [5]. Mice lacking the neurofilament medium subunit show axonal atrophy without significant motor neuron loss, and reduce contents of neurofilament light subunit [28]. Mice without the neurofilament heavy subunit also exhibit axonal atrophy without significant motor neuron loss [47]. Therefore, model mice lacking any of the neurofilament triplet protein subunits are not compatible with human ALS patients, as no significant motor neuron loss is evident.

Transgenic mice expressing the human wild-type neurofilament gene

Transgenic mice expressing the human wild-type neurofilament heavy chain gene show defective axonal transport and axonal atrophy in association with ultrastructural diminution of cytoskeletal components, the smooth endoplasmic reticulum, and mitochondria [16]. In mice showing a high level of expression, neurofilament aggregation is observed in the cytoplasm of neurons and proximal axons [17]. However, this transgenic mouse model shows no significant motor neuron loss [16]. Like neurofilament heavy chain-type transgenic mice, the neurofilament light chain-type transgenic mice show accumulation of neurofilaments in the neurons and axonal degeneration without significant motor neuron loss [99]. Therefore, transgenic mouse models expressing the human wild-type neurofilament gene bear no histopathological resemblance to human ALS in terms of significant motor neuron loss.

Transgenic mice expressing the human mutant neurofilament light chain gene with the L394P

Transgenic mice expressing the human mutant neurofilament light chain gene with the L394P develop neurological symptoms of muscle weakness. Unlike mice expressing the human wild-type neurofilament gene, these mice show significant motor neuron loss [64]. From this viewpoint, this mouse model is closely similar to human ALS on the basis of neurofilament pathology, although in human ALS there is no mutation of the neurofilament light chain gene with L394P [27].

Transgenic mice expressing the peripherin gene

Peripherin is a 58-kDa type III intermediate filament protein, which has been reported to be a component of ubiquitinated inclusion bodies in motor neurons of ALS patients [39]. As the name "peripherin" indicates, the protein exists mainly in the peripheral nervous system, and only a small amount is expressed with a selective distribution in the central nervous system. Overexpression of peripherin in transgenic mice leads to loss of spinal cord anterior horn cells and formation of inclusions that are immunoreactive for peripherin [4].

Transgenic mice expressing the dynamitin gene

The dynein/dynactin-complex is a type of motor protein responsible for minus-end-directed movement along the microtubule and plays an important role in fast retrograde-related axonal transport. Supporting the hypothesis that impairment of retrograde axonal transport causes motor neuron death, point mutations of the p150 subunit of the dynactin gene have been reported in ALS patients [70]. Experimentally, on the basis of this retrograde axonal transport impairment theory, mice overexpressing dynamitin, which is a subunit of dynactin, have been produced, and these mice show disruption of the dynein/dynactin complex, leading to inhibition of retrograde axonal transport. Histologically, such dynamitin-overexpressing mice show motor neuron loss [63].

Concluding remarks

Human ALS pathology exhibits a variety of cytopathological features including Bunina bodies, SLIs/RHIs, LBHIs/Ast-HIs, and NFCIs in addition to motor neuron degeneration. Among various rodent models of ALS, rodents with mutant SOD1 recapitulate motor neuron degeneration and SOD1-immunoreactive LBHIs/Ast-HIs, both of them found in SOD1-mutated FALS patients. Even with these similarities, human ALS pathology is different from that of rodents carrying SOD1 mutation, because (1) ALS is not a single entity but rather a heterogeneous syndrome, (2) relevant anatomical structures are different between humans and rodents, and (3) human pathology generally deals with only the terminal stage of the disease. In spite of these differences, motor neuron degeneration in rodent models provides us with opportunities to analyze the motor neuron degeneration process in detail and even to test therapeutic attempts. It is necessary to be aware not only of the similarities but also of differences between these ALS models and human ALS, because they are complementary.

Acknowledgments This study was supported in part by a Grant-in-Aid for Scientific Research (c) from the Ministry of Education, Culture, Sports, Science and Technology of Japan (SK: 17500229), a Grant for Research on Psychiatric and Neurological Disease and Mental Health from the Ministry of Health, Labor and Welfare of Japan (SK), and a Grant from The Research Group on Development of Novel Therapeutics for ALS of the Ministry of Health, Labor and Welfare of Japan (SK).

References

1. Aoki M (2004) Amyotrophic lateral sclerosis: recent insights from transgenic animal models with SOD1 mutations. Rinsho Shinkeigaku 44:778–791
2. Aoki M, Kato S, Nagai M, Itoyama Y (2005) Development of a rat model of amyotrophic lateral sclerosis expressing a human SOD1 transgene. Neuropathology 25:365–370
3. Arai T, Hasegawa M, Akiyama H, Ikeda K, Nonaka T, Mori H, Mann D, Tsuchiya K, Yoshida M, Hashizume Y, Oda T (2006) TDP-43 is a component of ubiquitin-positive inclusions in frontotemporal lobar degeneration and amyotrophic lateral sclerosis. Biochem Biophys Res Commun 351:602–611
4. Beaulieu JM, Nguyen MD, Julien JP (1999) Late onset death of motor neurons in mice over-expressing wild-type peripherin. J Cell Biol 147:531–544
5. Beaulieu JM, Jacomy H, Julien JP (2000) Formation of intermediate filament protein aggregates with disparate effects in two transgenic mouse models lacking the neurofilament light subunit. J Neurosci 20:5321–5328
6. Beers DR, Henkel JS, Xiao Q, Zhao W, Wang J, Yen AA, Siklos L, McKercher SR, Appel SH (2006) Wild-type microglia extend survival in PU.1 knockout mice with familial amyotrophic lateral sclerosis. Proc Natl Acad Sci USA 103:16021–16026
7. Ben Hamida M, Hentati F, Ben Hamida C (1990) Hereditary motor system diseases (chronic juvenile amyotrophic lateral sclerosis). Conditions combining a bilateral pyramidal syndrome with limb and bulbar amyotrophy. Brain 113:347–363
8. Bendotti C, Carrì MT (2004) Lessons from models of SOD1-linked familial ALS. Trends Mol Med 10:393–400
9. Boillée S, Yamanaka K, Lobsiger CS, Copeland NG, Jenkins NA, Kassiotis G, Kollias G, Cleveland DW (2006) Onset and progression in inherited ALS determined by motor neurons and microglia. Science 312:1389–1392
10. Bruijn LI, Becher MW, Lee MK, Anderson KL, Jenkins NA, Copeland NG, Sisodia SS, Rothstein JD, Borchelt DR, Price DL, Cleveland DW (1997) ALS-linked SOD1mutant G85R mediates damage to astrocytes and promotes rapidly progressive disease with SOD1-containing inclusions. Neuron 18:327–338

11. Bruijn LI, Houseweart MK, Kato S, Anderson KL, Anderson SD,Ohama E, Reaume AG, Scott RW, Cleveland DW (1998) Aggregation and motor neuron toxicity of an ALS-linked SOD1 mutant independent from wild-type SOD1. Science 281:1851–1854
12. Bunina TL (1962) On intracellular inclusions in familial amyotrophic lateral sclerosis. Zh Nevropathol Psikhiatr Im S S Korsakova 62:1293–1299
13. Cai H, Lin X, Xie C, Laird FM, Lai C, Wen H, Chiang HC, Shim H, Farah MH, Hoke A, Price DL, Wong PC (2005) Loss of ALS2 function is insufficient to trigger motor neuron degeneration in knock-out mice but predisposes neurons to oxidative stress. J Neurosci 25:7567–7574
14. Cervenakova L, Protas II, Hirano A, Votiakov VI, Nedzved MK, Kolomiets ND, Taller I, Park KY, Sambuughin N, Gajdusek DC, Brown P, Goldfarb LG (2000) Progressive muscular atrophy variant of familial amyotrophic lateral sclerosis (PMA/ALS). J Neurol Sci 177:124–130
15. Charcot JM (1874) De la sclérose latérale amyotrophique. Prog Méd 2: 325–327, 341–342, 453–455
16. Collard JF, Côté F, Julien JP (1995) Defective axonal transport in a transgenic mouse model of amyotrophic lateral sclerosis. Nature 375:61–64
17. Côté F, Collard JF, Juien JP (1993) Progressive neuronopahty in transgenic mice expressing the human neurofilament heavy gene: a mouse model of amyotrophic lateral sclerosis. Cell 73:35–46
18. Cudkowicz ME, McKenna-Yasek D, Chen C, Hedley-Whyte ET, Brown RH Jr (1998) Limited corticospinal tract involvement in amyotrophic lateral sclerosis subjects with the A4V mutation in the copper/zinc superoxide dismutase gene. Ann Neurol 43:703–710
19. Dal Canto MC, Gurney ME (1995) Neuropathological changes in two lines of mice carrying a transgene for mutant human Cu, Zn SOD, and in mice overexpressing wild type human SOD: a model of familial amyotrophic lateral sclerosis (FALS). Brain Res 676:25–40
20. Dal Canto MC, Mourelatos Z, Gonatas NK, Chiu A, Gurney ME (1996) Neuropathological changes depend on transgene copy numbers in transgenic mice for mutant human Cu, Zn superoxide dismutase (SOD). In: Nakano I, Hirano A (eds) Amyotrophic lateral sclerosis. progress and perspectives in basic research and clinical application. XIth TMIN international symposium, Tokyo, international congress series 1104. Elsevier, Tokyo, pp 331–338
21. Dal Canto MC, Gurney ME (1997) A low expressor line of transgenic mice carrying a mutant human Cu, Zn superoxide dismutase (SOD1) gene develops pathological changes that most closely resemble those in human amyotrophic lateral sclerosis. Acta Neuropathol (Berl) 93:537–550
22. Deng HX, Hentati A, Tainer JA, Iqbal Z, Cayabyab A, Hung WY, Getzoff ED, Hu P, Herzfeldt B, Roos RP, Warner C, Deng G, Soriano E, Smyth C, Parge HE, Ahmed A, Roses AD, Hallewell RA (1993) Amyotrophic lateral sclerosis and structural defects in Cu, Zn superoxide dismutase. Science 261:1047–1051
23. Deng HX, Shi Y, Furukawa Y, Zhai H, Fu R, Liu E, Gorrie GH, Khan MS, Hung WY, Bigio EH, Lukas T, Dal Canto MC, O'Halloran TV, Siddique T (2006) Conversion to the amyotrophic lateral sclerosis phenotype is associated with intermolecular linked insoluble aggregates of SOD1 in mitochondria. Proc Natl Acad Sci USA 103:7142–7147
24. Devon RS, Helm JR, Rouleau GA, Leitner Y, Lerman-Sagie T, Lev D, Hayden MR (2003) The first nonsense mutation in alsin results in a homogeneous phenotype of infantile-onset ascending spastic paralysis with bulbar involvement in two siblings. Clin Genet 64:210–215
25. Devon RS, Orban PC, Gerrow K, Barbieri MA, Schwab C, Cao LP, Helm JR, Bissada N, Cruz-Aguado R, Davidson TL, Witmer J, Metzler M, Lam CK, Tetzlaff W, Simpson EM, McCaffery JM, El-Husseini AE, Leavitt BR, Hayden MR (2006) Als2-deficient mice exhibit disturbances in endosome trafficking associated with motor behavioral abnormalities. Proc Natl Acad Sci USA 103:9595–9600
26. Dickson DW, Josephs KA, Amador-Ortiz C (2007) TDP-43 in differential diagnosis of motor neuron disorders. Acta Neuropathol 114:71–79
27. Doble A, Kennel P (2000) Animal models of amyotrophic lateral sclerosis. Amyotroph Lateral Scler Other Motor Neuron Disord 1:301–312
28. Elder GA, Friedrich VL Jr, Bosco P, Kang C, Gourov A, Tu PH, Lee VM, Lazzarini RA (1998) Absence of the mid-sized neurofilament subunit decreases axonal calibers, levels of light neurofilament (NF-L), and neurofilament content. J Cell Biol 141:727–739
29. Eymard-Pierre E, Lesca G, Dollet S, Santorelli FM, di Capua M, Bertini E, Boespflug-Tanguy O (2002) Infantile-onset ascending hereditary spastic paralysis is associated with mutations in the alsin gene. Am J Hum Genet 71: 518–527
30. Eymard-Pierre E, Yamanaka K, Haeussler M, Kress W, Gauthier-Barichard F, Combes P, Cleveland DW, Boespflug-Tanguy O (2006) Novel missense mutation in ALS2 gene results in infantile ascending hereditary spastic paralysis. Ann Neurol 59:976–980
31. Friedlander RM, Brown RH, Gagliardini V, Wang J, Yuan J (1997) Inhibition of ICE slows ALS in mice. Nature 388:31
32. Fujimura H, Sumi H, Fukada K, Takayasu S, Sakoda S, Nakanishi T, Shimuzu A, Kato S (2002) Stability of mutant superoxide dismutase-1 and incidence of Lewy body-like hyaline inclusions in familial amyotrophic lateral sclerosis (in Japanese with English abstract) Rinsho Shinkeigaku 42:1283
33. Gascon GG, Chavis P, Yaghmour A, Stigsby B, Shums A, Ozand P, Siddique T (1995) Familial childhood primary lateral sclerosis with associated gaze paresis. Neuropediatrics 26:313–319
34. Gong YH, Parsadanian AS, Andreeva A, Snider WD, Elliott JL (2000) Restricted expression of G86R Cu/Zn superoxide dismutase in astrocytes results in astrocytosis but does not cause motoneuron degeneration. J Neurosci 20:660–665
35. Gros-Louis F, Meijer IA, Hand CK, Dubé MP, MacGregor DL, Seni MH, Devon RS, Hayden MR, Andermann F, Andermann E, Rouleau GA (2003) An ALS2 gene mutation causes hereditary spastic paraplegia in a Pakistani kindred. Ann Neurol 53:144–145
36. Gurney ME, Pu H, Chiu AY, Dal Canto MC, Polchow CY, Alexander DD, Caliendo J, Hentati A, Kwon YW, Deng H-X, Chen W, Zhai P, Sufit RL, Siddique T (1994) Motor neuron degeneration in mice that express a human Cu, Zn superoxide dismutase mutation. Science 264:1772–1775
37. Hadano S, Hand CK, Osuga H, Yanagisawa Y, Otomo A, Devon RS, Miyamoto N, Showguchi-Miyata J, Okada Y, Singaraja R, Figlewicz DA, Kwiatkowski T, Hosler BA, Sagie T, Skaug J, Nasir J, Brown RH Jr, Scherer SW, Rouleau GA, Hayden MR, Ikeda JE (2001) A gene encoding a putative GTPase regulator is mutated in familial amyotrophic lateral sclerosis 2. Nat Genet 29:166–173
38. Hadano S, Benn SC, Kakuta S, Otomo A, Sudo K, Kunita R, Suzuki-Utsunomiya K, Mizumura H, Shefner JM, Cox GA, Iwakura Y, Brown RH Jr, Ikeda JE (2006) Mice deficient in the Rab5 guanine nucleotide exchange factor ALS2/alsin exhibit age-dependent neurological deficits and altered endosome trafficking. Hum Mol Genet 15:233–250
39. He CZ, Hays AP (2004) Expression of peripherin in ubiquitinated inclusions of amyotrophic lateral sclerosis. J Neurol Sci 217:47–54
40. Higgins CMJ, Jung C, Xu Z (2003) ALS-associated mutant $SOD1^{G93A}$ causes mitochondrial vacuolation by expansion of the intermembrane space and by involvement of SOD1 aggregation and peroxisomes. BMC Neurosci 4:16

41. Hirano A (1965) Pathology of amyotrophic lateral sclerosis. In: Gajdusek DC, Gibbs CJ Jr, Alpers MP (eds) Slow, latent, and temperate virus infections. NINDB Monograph No.2 Washington: U.S. National Institute of Neurological Diseases and Blindness, National Institute of Health (U.S.), pp 23–37
42. Hirano A, Kurland LT, Sayre GP (1967) Familial amyotrophic lateral sclerosis. A subgroup characterized by posterior and spinocerebellar tract involvement and hyaline inclusions in the anterior horn cells. Arch Neurol 16:232–243
43. Howland DS, Liu J, She Y, Goad B, Maragakis NJ, Kim B, Erickson J, Kulik J, DeVito L, Psaltis G, DeGennaro LJ, Cleveland DW, Rothstein JD (2002) Focal loss of the glutamate transporter EAAT2 in a transgenic rat model of SOD1 mutant-mediated amyotrophic lateral sclerosis (ALS). Proc Natl Acad Sci USA 99:1604–1609
44. Ince PG, Shaw PJ, Slade JY, Jones C, Hudgson P (1996) Familial amyotrophic lateral sclerosis with a mutation in exon 4 of the Cu/Zn superoxide dismutase gene: pathological and immunocytochemical changes. Acta Neuropathol 92:395–403
45. Ince PG, Tomkins J, Slade JY, Thatcher NM, Shaw PJ (1998) Amyotrophic lateral sclerosis associated with genetic abnormalities in the gene encoding Cu/Zn superoxide dismutase: molecular pathology of five new cases, and comparison with previous reports and 73 sporadic cases of ALS. J Neuropathol Exp Neurol 57:895–904
46. Inoue K, Fujimura H, Ogawa Y, Satoh T, Shimada K, Sakoda S (2002) Familial amyotrophic lateral sclerosis with a point mutation (G37R) of the superoxide dismutase 1 gene: a clinicopathological study. Amyotroph Lateral Scler Other Motor Neuron Disord 3:244–247
47. Jacomy H, Zhu Q, Couillard-Després S, Beaulieu JM, Julien JP (1999) Disruption of type IV intermediate filament network in mice lacking the neurofilament medium and heavy subunits. J Neurochem 73:972–984
48. Jonsson PA, Ernhill K, Andersen PM, Bergemalm D, Brännström T, Gredal O, Nilsson P, Marklund SL (2004) Minute quantities of misfolded mutant superoxide dismutase-1 cause amyotrophic lateral sclerosis. Brain 127:73–88
49. Jonsson PA, Graffmo KS, Brännström T, Nilsson P, Andersen PM, Marklund SL (2006) Motor neuron disease in mice expressing the wild type-like D90A mutant superoxide dismutase-1. J Neuropathol Exp Neurol 65:1126–1136
50. Kadekawa J, Fujimura H, Yanagihara T, Sakoda S (2001) A clinicopathological study of patient with familial amyotrophic lateral sclerosis associated with a two-base pair deletion in the copper/zinc superoxide dismutase (SOD1) gene. Acta Neuropathol 101:415
51. Katayama S, Watanabe C, Noda K, Ohishi H, Yamamura Y, Nishisaka T, Inai K, Asayama K, Murayama S, Nakamura S (1999) Numerous conglomerate inclusions in slowly progressive familial amyotrophic lateral sclerosis with posterior column involvement. J Neurol Sci 171:72–77
52. Kato M, Kato S, Abe Y, Nishino T, Ohama E, Aoki M, Itoyama Y (2006) Histological recovery of the hepatocytes is based on the redox system upregulation in the animal models of mutant superoxide dismutase (SOD)1-linked amyotrophic lateral sclerosis. Histol Histopathol 21:729–742
53. Kato S, Shimoda M, Watanabe Y, Nakashima K, Takahashi K, Ohama E (1996) Familial amyotrophic lateral sclerosis with a two base pair deletion in superoxide dismutase 1 gene: multisystem degeneration with intracytoplasmic hyaline inclusions in astrocytes. J Neuropathol Exp Neurol 55:1089–1101
54. Kato S, Hayashi H, Nakashima K Nanba E, Kato M, Hirano A, Nakano I, Asayama K, Ohama E (1997) Pathological characterization of astrocytic hyaline inclusions in familial amyotrophic lateral sclerosis. Am J Pathol 151:611–620
55. Kato S, Saito M, Hirano A, Ohama E (1999) Recent advances in research on neuropathological aspects of familial amyotrophic lateral sclerosis with superoxide dismutase 1 gene mutations: neuronal Lewy body-like hyaline inclusions and astrocytic hyaline inclusions. Histol Histopathol 14:973–989
56. Kato S, Horiuchi S, Liu J, Cleveland DW, Shibata N, Nakashima K, Nagai R, Hirano A, Takikawa M, Kato M, Nakano I, Ohama E (2000) Advanced glycation endproduct-modified superoxide dismutase-1 (SOD1)-positive inclusions are common to familial amyotrophic lateral sclerosis patients with SOD1 gene mutations and transgenic mice expressing human SOD1 with a G85R mutation. Acta Neuropathol 100:490–505
57. Kato S, Takikawa M, Nakashima K, Hirano A. Cleveland DW, Kusaka H, Shibata N, Kato M, Nakano I, Ohama E (2000) New consensus research on neuropathological aspects of familial amyotrophic lateral sclerosis with superoxide dismutase 1 (SOD1) gene mutations: Inclusions containing SOD1 in neurons and astrocytes. Amyotroph Lateral Scler Other Motor Neuron Disord 1:163–184
58. Kato S, Shaw P, Wood-Allum C, Leigh PN, Show C (2003) Amyotrophic lateral sclerosis. In: Dickson DW (ed) Neurodegeneration: the molecular pathology of dementia and movement disorders. ISN Neuropath, Basel, pp 350–368
59. Kato S, Kato M, Abe Y, Matsumura T, Nishino T, Aoki M, Itoyama Y, Asayama K, Awaya A, Hirano A, Ohama E (2005) Redox system expression in the motor neurons in amyotrophic lateral sclerosis (ALS): immunohistochemical studies on sporadic ALS, superoxide dismutase 1 (SOD1)-mutated familial ALS, and SOD1-mutated ALS animal models. Acta Neuropathol 110:101–112
60. Kokubo Y, Kuzuhara S, Narita Y, Kikugawa K, Nakano R, Inuzuka T, Tsuji S, Watanabe M, Miyazaki T, Murayama S, Ihara Y (1999) Accumulation of neurofilaments and SOD1-immunoreactive products in a patient with familial amyotrophic lateral sclerosis with I113T SOD1 mutation. Arch Neurol 56:1506–1508
61. Kong J, Xu Z (1998) Massive mitochondrial degeneration in motor neurons triggers the onset of amyotrophic lateral sclerosis in mice expressing a mutant SOD1. J Neurosci 18:3241–3250
62. Kress JA, Kühnlein P, Winter P, Ludolph AC, Kassubek J, Müller U, Sperfeld AD (2005) Novel mutation in the ALS2 gene in juvenile amyotrophic lateral sclerosis. Ann Neurol 58:800–803
63. LaMonte BH, Wallace KE, Holloway BA, Shelly SS, Ascaño J, Tokito M, Van Winkle T, Howland DS, Holzbaur EL (2002) Disruption of dynein/dynactin inhibits axonal transport in motor neurons causing late-onset progressive degeneration. Neuron 34:715–727
64. Lee MK, Marszalek JR, Cleveland DW (1994) A mutant neurofilament subunit causes massive, selective motor neuron death: implications for the pathogenesis of human motor neuron disease. Neuron 13:975–988
65. Lino MM, Schneider C, Caroni P (2002) Accumulation of SOD1 mutants in postnatal motoneurons does not cause motoneuron pathology or motoneuron disease. J Neurosci 22:4825–4832
66. Miller TM, Kim SH, Yamanaka K, Hester M, Umapathi P, Arnson H, Rizo L, Mendell JR, Gage FH, Cleveland DW, Kaspar BK (2006) Gene transfer demonstrates that muscle is not a primary target for non-cell-autonomous toxicity in familial amyotrophic lateral sclerosis. Proc Natl Acad Sci USA 103:19546–19551
67. Mochizuki Y, Mizutani T, Nakano R, Fukushima T, Honma T, Nemoto N, Takei K (2003) Clinical features and neuropathological findings of familial amyotrophic lateral sclerosis with an H43R mutation in Cu/Zn superoxide dismutase. Rinsho Shinkeigaku 43:491–449
68. Morrison BM, Gordon JW, Ripps ME, Morrison JH (1996) Quantitative immunocytochemical analysis of the spinal cord in G86R superoxide dismutase transgenic mice: neurochemical correlates of selective vulnerability. J Comp Neurol 373:619–631

69. Mourelatos Z, Gonatas NK, Stieber A, Gurney ME, Dal Canto MC (1996) The Golgi apparatus of spinal cord motor neurons in transgenic mice expressing mutant Cu, Zn superoxide dismutase becomes fragmented in early, preclinical stages of the disease. Proc Natl Acad Sci USA 93:5472–5477
70. Münch C, Sedlmeier R, Meyer T, Homberg V, Sperfeld AD, Kurt A, Prudlo J, Peraus G, Hanemann CO, Stumm G, Ludoph AC (2004) Point mutations of the p150 subunit of dynactin (DCTN1) gene in ALS. Neurology 63:724–726
71. Murayama S, Namba E, Nishiyama, Kitamura Y, Morita T, Nakashima K, Ishida T, Mizutani T, Kanazawa I (1997) Molecular pathological studies of familial amyotrophic lateral sclerosis. Neuropathology 17(Suppl):219
72. Nagai M, Aoki M, Miyoshi I, Kato M, Pasinelli P, Kasai N, Brown RH Jr, Itoyama Y (2001) Rats expressing human cytosolic copper-zinc superoxide dismutase transgenes with amyotrophic lateral sclerosis: associated mutations develop motor neuron disease. J Neurosci 21:9246–9254
73. Nagai M, Re DB, Nagata T, Chalazonitis A, Jessell TM, Wichterle H, Przedborski S (2007) Astrocytes expressing ALS-linked mutated SOD1 release factors selectively toxic to motor neurons. Nat Neurosci 10:615–622
74. Neumann M, Sampathu DM, Kwong LK, Truax A, Micsenyi MC, Chou TT, Bruce J, Schuck T, Grossman M, Clark CM, McCluskey LF, Miller BL, Masliah E, Mackenzie IR, Feldman H, Feiden W, Kretzschmar HA, Trojanowski JQ, Lee VM-Y (2006) Ubiquitinated TDP-43 in frontotemporal lobar degeneration and amyotrophic lateral sclerosis. Science 314:130–133
75. Nimchinsky EA, Young WG, Yeung G, Shah RA, Gordon JW, Bloom FE, Morrison JH, Hof PR (2000) Differential vulnerability of oculomotor, facial, and hypoglossal nuclei in G86R superoxide dismutase transgenic mice. J Comp Neurol 416:112–125
76. Ohi T, Nabeshima K, Kato S, Yazawa S, Takechi S (2004) Familial amyotrophic lateral sclerosis with His46Arg mutation in Cu/Zn superoxide dismutase presenting characteristic clinical features and Lewy body-like hyaline inclusions. J Neurol Sci 225: 19–25
77. Ohtsubo M, Kai R, Furuno N, Sekiguchi T, Sekiguchi M, Hayashida H, Kuma K, Miyata T, Fukushige S, Murotsu T (1987) Isolation and characterization of the active cDNA of the human cell cycle gene (RCC1) involved in the regulation of onset of chromosome condensation. Genes Dev 1:585–593
78. Orrell RW, King AW, Hilton DA, Campbell MJ, Lane RJM, de Belleroche JS (1995) Familial amyotrophic lateral sclerosis with a point mutation of SOD-1: intrafamilial heterogeneity of disease duration associated with neurofibrillary tangles. J Neurol Neurosurg Psychiatry 59:266–270
79. Otomo A, Hadano S, Okada T, Mizumura H, Kunita R, Nishijima H, Showguchi-Miyata J, Yanagisawa Y, Kohiki E, Suga E, Yasuda M, Osuga H, Nishimoto T, Narumiya S, Ikeda JE (2003) ALS2, a novel guanine nucleotide exchange factor for the small GTPase Rab5, is implicated in endosomal dynamics. Hum Mol Genet 12:1671–1687
80. Pramatarova A, Laganière J, Roussel J, Brisebois K, Rouleau GA (2001) Neuron-specific expression of mutant superoxide dismutase 1 in transgenic mice does not lead to motor impairment. J Neurosci 21:3369–3374
81. Ripps ME, Huntley GW, Hof PR, Morrison JH, Gordon JW (1995) Transgenic mice expressing an altered murine superoxide dismutase gene provide an animal model of amyotrophic lateral sclerosis. Proc Natl Acad Sci USA 92:689–693
82. Robertson J, Kriz J, Nguyen MD, Julien JP (2002) Pathways to motor neuron degeneration in transgenic mouse models. Biochimie 84:1151–1160
83. Robertson J, Sanelli T, Xiao S, Yang W, Horne P, Hammond R, Pioro EP, Strong MJ (2007) Lack of TDP-43 abnormalities in mutant SOD1 transgenic mice shows disparity with ALS. Neurosci Lett 420:128–132
84. Rosen DR, Siddique T, Patterson D, Figlewicz DA, Sapp P, Hentati A, Donaldson D, Goto J, O'Regan JP, Deng HX, Rahmani Z, Krizus A, McKenna-Yasek D, Cayabyab A, Gaston SM, Berger R, Tanzi RE, Halperin JJ, Herzfeldt B, Van den Bergh R, Hung-WY, Bird T, Deng G, Mulder DW, Smyth C, Laing NG, Soriano E, Pericak-Vance MA, Haines J, Rouleau GA, Gusella JS, Horvitz HR, Brown RH (1993) Mutations in Cu/Zn superoxide dismutase gene are associated with familial amyotrophic lateral sclerosis. Nature 362:59–62
85. Rouleau GA, Clark AW, Rooke K, Pramatarova A, Krizus A, Suchowersky O, Julien JP, Figlewicz D (1996) SOD1 mutation is associated with accumulation of neurofilaments in amyotrophic lateral sclerosis. Ann Neurol 39:128–131
86. Sato T, Nakanishi T, Yamamoto Y, Andersen PM, Ogawa Y, Fukada K, Zhou Z, Aoike F, Sugai F, Nagano S, Hirata S, Ogawa M, Nakano R, Ohi T, Kato T, Nakagawa M, Hamasaki T, Shimizu A, Sakoda S (2005) Rapid disease progression correlates with instability of mutant SOD1 in familial ALS. Neurology 65:1854–1860
87. Schmidt A, Hall A (2002) Guanine nucleotide exchange factors for Rho GTPases: turning on the switch. Genes Dev 16:1587–1609
88. Shaw CE, Enayat ZE, Powell JF, Anderson VER, Radunovic A, al-Sarraj S, Leigh PN (1997) Familial amyotrophic lateral sclerosis: molecular pathology of a patient with a SOD1 mutation. Neurology 49:1612–1616
89. Shibata N, Hirano A, Kobayashi M, Siddique T, Deng HX, Hung WY, Kato T, Asayama K (1996) Intense superoxide dismutase-1 immunoreactivity in intracytoplasmic hyaline inclusions of familial amyotrophic lateral sclerosis with posterior column involvement. J Neuropathol Exp Neurol 55:481–490
90. Stieber A, Gonatas JO, Gonatas NK (2000) Aggregation of ubiquitin and a mutant ALS-linked SOD1 protein correlate with disease progression and fragmentation of the Golgi apparatus. J Neurol Sci 173: 53–62
91. Sumi H, Nagano S, Fujimura H, Kato S, Sakoda S (2006) Inverse correlation between the formation of mitochondria-derived vacuoles and Lewy-body-like hyaline inclusions in G93A superoxide-dismutase-transgenic mice. Acta Neuropathol 112:52–63
92. Takahashi H, Makifuchi T, Nakano R, Sato S, Inuzuka T, Sakimura K, Mishina M, Honma Y, Tsuji S, Ikuta F (1994) Familial amyotrophic lateral sclerosis with a mutation in the Cu/Zn superoxide dismutase gene. Acta Neuropathol 88:185–188
93. Takehisa Y, Ujike H, Ishizu H, Terada S, Haraguchi T, Tanaka Y, Nishinaka T, Nobukuni K, Ihara Y, Namba R, Yasuda T, Nishibori M, Hayabara T, Kuroda S (2001) Familial amyotrophic lateral sclerosis with a novel Leu126Ser mutation in the copper/zinc superoxide dismutase gene showing mild clinical features and Lewy body-like hyaline inclusions. Arch Neurol 58:736–740
94. Tan CF, Piao YS, Hayashi S, Obata H, Umeda Y, Sato M, Fukushima T, Nakano R, Tsuji S, Takahashi H (2004) Familial amyotrophic lateral sclerosis with bulbar onset and a novel Asp101Tyr Cu/Zn superoxide dismutase gene mutation. Acta Neuropathol 108:332–336
95. Tan CF, Eguchi H, Tagawa A, Onodera O, Iwasaki T, Tsujino A, Nishizawa M, Kakita A, Takahashi H (2007) TDP-43 immunoreactivity in neuronal inclusions in familial amyotrophic lateral sclerosis with or without SOD1 gene mutation. Acta Neuropathol 113:535–542
96. Wang J, Xu G, Gonzales V, Coonfield M, Fromholt D, Copeland NG, Jenkins NA, Borchelt DR (2002) Fibrillar inclusions and motor neuron degeneration in transgenic mice expressing superoxide dismutase 1 with a disrupted copper-binding site. Neurobiol Dis 10:128–138

97. Watanabe Y, Yasui K, Nakano T, Doi K, Fukada Y, Kitayama M, Ishimoto M, Kurihara S, Kawashima M, Fukuda H, Adachi Y, Inoue T, Nakashima K (2005) Mouse motor neuron disease caused by truncated SOD1 with or without C-terminal modification. Mol Brain Res 135:12–20
98. Wong PC, Pardo CA, Borchelt DR, Lee MK, Copeland NG, Jenkins NA, Sisodia SS, Cleveland DW, Price DL (1995) An adverse property of a familial ALS-linked SOD1 mutation causes motor neuron disease characterized by vacuolar degeneration of mitochondria. Neuron 14:1105–1116
99. Xu Z, Cork LC, Griffin JW, Cleveland DW (1993) Increased expression of neurofilament subunit NF-L produces morphological alterations that resemble the pathology of human motor neuron disease. Cell 73:23–33
100. Yamagishi S, Koyama Y, Katayama T, Taniguchi M, Hitomi J, Kato M, Aoki M, Itoyama Y, Kato S, Tohyama M (2007) An in vitro model for Lewy body-like hyaline inclusion/astrocytic hyaline inclusion: induction by ER stress with an ALS-linked SOD1 mutation. PLoS One 2:e1030
101. Yamanaka K, Miller TM, McAlonis-Downes M, Chun SJ, Cleveland DW (2006) Progressive spinal axonal degeneration and slowness in ALS2-deficient mice. Ann Neurol 60:95–104
102. Yang Y, Hentati A, Deng HX, Dabbagh O, Sasaki T, Hirano M, Hung WY, Ouahchi K, Yan J, Azim AC, Cole N, Gascon G, Yagmour A, Ben-Hamida M, Pericak-Vance M, Hentati F, Siddique T (2001) The gene encoding alsin, a protein with three guanine-nucleotide exchange factor domains, is mutated in a form of recessive amyotrophic lateral sclerosis. Nat Genet 29:160–165
103. Zang DW, Cheema SS (2002) Degeneration of corticospinal and bulbospinal systems in the superoxide dismutase $1^{G93A\,G1H}$ transgenic mouse model of familial amyotrophic lateral sclerosis. Neurosci Lett 332:99–102

An *In Vitro* Model for Lewy Body-Like Hyaline Inclusion/ Astrocytic Hyaline Inclusion: Induction by ER Stress with an ALS-Linked SOD1 Mutation

Satoru Yamagishi[1,2*☯¤a], Yoshihisa Koyama[1,2☯], Taiichi Katayama[1,2☯¤b], Manabu Taniguchi[1,2], Junichi Hitomi[1,2], Masaaki Kato[3], Masashi Aoki[3], Yasuto Itoyama[3], Shinsuke Kato[4*], Masaya Tohyama[1,2]

1 Department of Anatomy and Neuroscience, Graduate School of Medicine, Osaka University, Suita, Osaka, Japan, 2 The 21st Century Center of Excellence Program, Graduate School of Medicine, Osaka University, Suita, Osaka, Japan, 3 Department of Neurology, Tohoku University School of Medicine, Sendai, Japan, 4 Department of Neuropathology, Institute of Neurological Sciences, Faculty of Medicine, Tottori University, Yonago, Japan

Neuronal Lewy body-like hyaline inclusions (LBHI) and astrocytic hyaline inclusions (Ast-HI) containing mutant Cu/Zn superoxide dismutase 1 (SOD1) are morphological hallmarks of familial amyotrophic lateral sclerosis (FALS) associated with mutant SOD1. However, the mechanisms by which mutant SOD1 contributes to formation of LBHI/Ast-HI in FALS remain poorly defined. Here, we report induction of LBHI/Ast-HI-like hyaline inclusions (LHIs) *in vitro* by ER stress in neuroblastoma cells. These LHI closely resemble LBHI/Ast-HI in patients with SOD1-linked FALS. LHI and LBHI/Ast-HI share the following features: 1) eosinophilic staining with a pale core, 2) SOD1, ubiquitin and ER resident protein (KDEL) positivity and 3) the presence of approximately 15–25 nm granule-coated fibrils, which are morphological hallmark of mutant SOD1-linked FALS. Moreover, in spinal cord neurons of L84V SOD1 transgenic mice at presymptomatic stage, we observed aberrant aggregation of ER and numerous free ribosomes associated with abnormal inclusion-like structures, presumably early stage neuronal LBHI. We conclude that the LBHI/Ast-HI seen in human patients with mutant SOD1-linked FALS may arise from ER dysfunction.

Citation: Yamagishi S, Koyama Y, Katayama T, Taniguchi M, Hitomi J, et al (2007) An *In Vitro* Model for Lewy Body-Like Hyaline Inclusion/Astrocytic Hyaline Inclusion: Induction by ER Stress with an ALS-Linked SOD1 Mutation. PLoS ONE 2(10): e1030. doi:10.1371/journal.pone.0001030

INTRODUCTION

Amyotrophic lateral sclerosis (ALS) is a progressive neurodegenerative disorder in which both upper and lower motor neurons begin to degenerate in middle-aged persons. About 10% of ALS patients demonstrate autosomal dominant inheritance of this disease, a disorder known as familial ALS (FALS) [1–6]. About 20% of FALS cases are associated with mutations of the Cu/Zn-superoxide dismutase (SOD1) gene [7]. SOD1 is an abundant protein of approximately 153 amino acids that accounts for approximately 1% of total cytosolic protein. More than 100 different SOD1 mutations have been reported as risk factors in association with FALS.

The endoplasmic reticulum (ER) is responsible for the synthesis, initial post-translational modification, and proper folding of proteins, as well as for their sorting export and delivery to appropriate cellular destinations. A variety of conditions, such as loss of the intraluminal oxidative environment or loss of calcium homeostasis, can cause accumulation of misfolded proteins in the ER. To cope with such accumulation, there are three possible responses in eukaryotes. The first response is known as the unfolded protein response (UPR), in which IRE1α and ATF6 recognize aberrant proteins and increase the expression of ER-resident chaperones such as GRP78/BiP and GRP94 to promote proper protein folding [8,9]. The second response involves suppression of translation mediated by the serine/threonine kinase PERK, which phosphorylates and inactivates the translation initiation factor eIF-2α to reduce the production of misfolded proteins [10,11]. The third response is ER-associated degradation (ERAD), in which misfolded proteins are expelled from the ER and targeted for degradation by cytoplasmic proteasomes [12,13]. Although these three protective responses can transiently control the accumulation of misfolded proteins within the ER, they can be overcome by sustained 'ER stress' [14–16]. 'ER stress' is involved in neuronal death and various neurodegenerative disorders, such as Charcot-Marie-Tooth disease, and is especially related to inclusion body diseases such as Alzheimer's disease, Parkinson's disease, Huntington's disease and ALS [17–23].

Histopathologic studies have revealed that neuronal Lewy body-like hyaline inclusions (LBHI) and astrocytic hyaline inclusions (Ast-HI), are morphological hallmarks of mutant SOD1-linked FALS [24]. Neuronal LBHI and Ast-HI are ultrastructually identical and share various features, with both consisting of 15–25 nm granule-coated fibrils, both showing immunoreactivity for

Academic Editor: Xiao-Jiang Li, Emory University, United States of America

Received February 28, 2007; **Accepted** September 23, 2007; **Published** October 10, 2007

Funding: This work was supported in part by a grant from the 21st Century COE Program, Japan Society for the Promotion of Science, 6 Ichibancho, Chiyoda-ku, Tokyo 102-8471, Japan, a Grant-in-Aid for Scientific Research (c) from the Ministry of Education, Culture, Sports, Science and Technology of Japan (S.K.: 17500229), a Grant from Research on Psychiatric and Neurological Disease and Mental Health (SK, MA, YI) and a Research Grant on Measures for Intractable Diseases from the Ministry of Health, Labour and Welfare of Japan (SK, YI). SY is supported by a long-term fellowship by European Molecular Biology Organization (EMBO) and Japan Society for the Promotion of Science (JSPS).

Competing Interests: The authors have declared that no competing interests exist.

* **To whom correspondence should be addressed.** E-mail: yamagishi@neuro.mpg.de (SY); kato@grape.med.tottori-u.ac.jp (SK)

☯ These authors contributed equally to this work.

¤a **Current address:** Molecular Neurobiology, Max-Planck-Institute of Neurobiology, Martinsried, Munich, Germany,
¤b **Current address:** Department of Anatomy and Neuroscience, Hamamatsu University School of Medicine, Hamamatsu, Shizuoka, Japan

SOD1, ubiquitin, and copper chaperone for SOD (CCS), and both appearing late in the course of the disease (i.e. at ~10 to 30 years of age in humans [24–27]). Recently, Wate et al. reported that neuronal LBHI are immunoreactive for GRP78/BiP, a component of the UPR cellular response to ER stress [28].

In the present study, we show that ER stress in a neuroblastoma line expressing mutant SOD1 can provoke SOD1 aggregation in ER and formation of LBHI/Ast-HI-like hyaline inclusion bodies (LHIs), which show SOD1, ubiquitin, GRP78/BiP and ER resident protein (KDEL) immunopositivity similar to the shared cytopathological features of LBHI and Ast-HI. Induced neuroblastoma LHI furthermore consisted of 15–25 nm granule-coated fibrils, a hallmark of mutant SOD1-linked FALS, raising the possibility that these acutely induced aggregations represent a precursor to LBHI/Ast-HI seen in advanced FALS. In support of this possibility, we observe abnormal ER and numerous free ribosomes aggregated in the peri-nuclear region neuroblastoma cells expressing L84V SOD1 under ER stress condition and in spinal cord neurons in presymptomatic transgenic mice expressing L84V SOD1. Taken together, these findings suggest a model for early events in FALS cellular pathology, in which ER stress promotes the aggregation of mutant SOD1 and is involved in the development of LBHI/Ast-HI in patients with mutant SOD1 linked FALS.

RESULT

Aggregation and ubiquitination of mutant SOD1 under ER stress

To identify conditions which lead to the aggregation of mutant SOD1, we generated SK-N-SH human neuroblastoma cell lines that stably expressed FLAG-tagged human SOD1 encoding a leucine to valine substitution mutation (L84V) associated with FALS [29]. Western blot analysis confirmed that expression of endogenous and exogenous SOD1 was equal in the cell line (Fig. 1A). Reports that neuronal LBHI contain GRP78/BiP, an ER resident component of the UPR response, suggested that ER stress might be a factor in the aggregation of mutant SOD1 [28]. We therefore examined localization of wild-type and mutant SOD1 under normal conditions and under conditions of ER stress (Figure 1). Under normal conditions, wild-type and L84V SOD1 were distributed through the cytosol (Fig. 1B and D). However, following treatment with tunicamycin, an inhibitor of N-glycosylation which causes ER stress, small SOD1-positive aggregates (up to 3 μm in diameter) were seen in L84V SOD1-expressing cells (22.3%, $p<0.001$; Fig. 1E and F). A much smaller percentage of wild-type SOD1 expressing cells (2.9%, n.s.) showed non-inducible SOD1 aggregation (Fig. 1C and F). To confirm whether ER stress is required for the aggregation of SOD1, we compared tunicamycin and thapsigargin as ER stress inducers with etoposide as a non-ER stress inducer (causing DNA damage). Exposure to 1 and 3 μg/ml tunicamycin (21.1% and 17.5%, respectively) or 0.3 and 1 μM thapsigargin (27.0% and 27.2%, respectively) significantly increased the number of cells containing SOD1 aggregates, in L84V SOD1 expressing neuroblastoma cells. Treatment with 100 and 300 μM etoposide did not lead to a significant increase in aggregates (Fig. 1G). Thus mutant SOD1 forms aggregates following treatments provoking ER stress, but not following treatment causing damage to the nucleus.

Since the SOD1-positive inclusions of FALS patients are known to be eosinophilic [26], we performed hematoxylin-eosin (HE) and anti-SOD1 antibody staining to determine whether the aggregates induced in the neuroblastoma line were also eosinophilic.

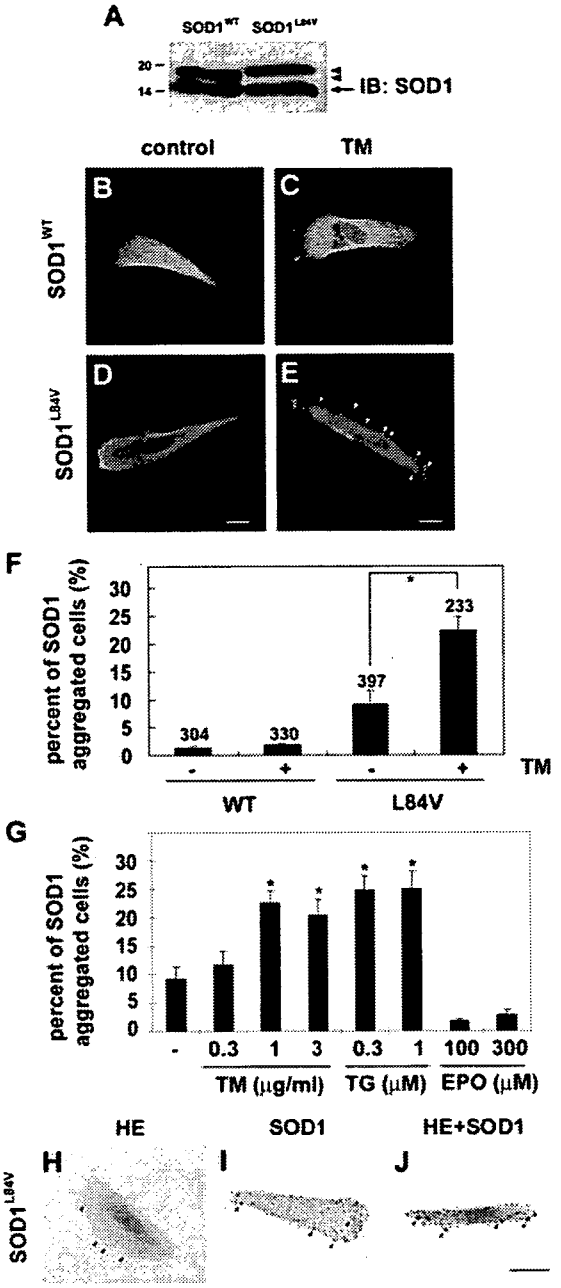

Figure 1. Eosinophilic aggregates of L84V SOD1 are induced by ER stress. (A) Western blotting analysis of the expression of SOD1 in SK-N-SH cells, which stably expressed FLAG tagged wild-type SOD1 or L84V mutant SOD1. Arrowheads and arrow indicate exogenous and endogenous SOD1, respectively. (B–D) Immunofluorescent analysis of SOD1 aggregates in SK-N-SH cells expressing wild-type SOD1 (B, C) or L84V SOD1 (D, E). Cells were incubated under control conditions (B, D) or with 1 μg/ml tunicamycin (C, E) for 24 h, and then were fixed and stained with an anti-SOD1 antibody. Tunicamycin induced aggregates of SOD1 (arrowheads) in L84V SOD1-expressing cells, but not in wild-type SOD1-expressing cells. Scale bar = 20 μm. (F) Quantification of (B-D). After the staining the cells with SOD1 aggregates were counted and scored. Numbers indicate the amounts of total counted cells. Asterisks show a significant difference from control, *$p<0.001$. (G) SOD1 aggregates induced by tunicamycin and thapsigargin, but not by etoposide. SK-N-SH cells expressing L84V SOD1 were exposed to 0.3, 1 and 3 μg/ml tunicamycin, 0.3 and 1 μM thapsigargin and 100 and 300 μM etoposide. Asterisks show a significant difference from control, *$p<0.001$. (H-J) Eosinophilic SOD1 aggregates induced by tunicamycin. Cells were treated as described in (E) and then stained with HE (H), anti-SOD1 antibody (I), or both (J). Scale bar = 20 μm.
doi:10.1371/journal.pone.0001030.g001

Figures 1H–J show that the aggregates induced by tunicamycin treatment were positive for both eosin and SOD1.

In patients with mutant SOD1-linked FALS, SOD1-positive aggregates are reported to be ubiquitinated by RING finger-type E3 ubiquitin ligases such as dorfin [30–33]. To investigate whether the SOD1 aggregates induced by ER stress were ubiquitinated, we performed double immunostaining with anti-SOD1 and anti-ubiquitin antibodies (Fig. 2 A–R). After treatment with either tunicamycin or ALLN, a specific proteasome inhibitor, wild-type and L84V SOD1-expressing cells were immunostained with anti-SOD1 and anti-ubiquitin antibodies. As a result, mutant SOD1 aggregates induced by either tunicamycin or ALLN were clearly colocalized with ubiquitin, suggesting the SOD1 were ubiquitinated. To further examine the ubiquitination of the mutant SOD1, a co-immunoprecipitation assay utilizing ubiquitin was performed (Fig. 2S). As expected, L84V SOD1-expressing cells showed a positive ubiquitin ladder after ALLN treatment, but wild-type SOD1-expressing cells did not.

Aggregates of SOD1 show positive localization to the ER, but not to the mitochondria, lysosomes, or Golgi apparatus

Under normal conditions, SOD1 is diffusely distributed throughout the cytoplasm. In contrast, under the pathological condition, SOD1 aggregates are associated with specific organelles such as the mitochondria and/or ER [34–37]. Since the tunicamycin-induced aggregates of mutant SOD1 were localized to the central and peripheral regions of the cytoplasm (Fig. 1E, H–J), we investigated the subcellular localization of these aggregates with organelle specific markers. Confocal microscopy analysis clearly showed colocalization of SOD1 and an ER retention signal

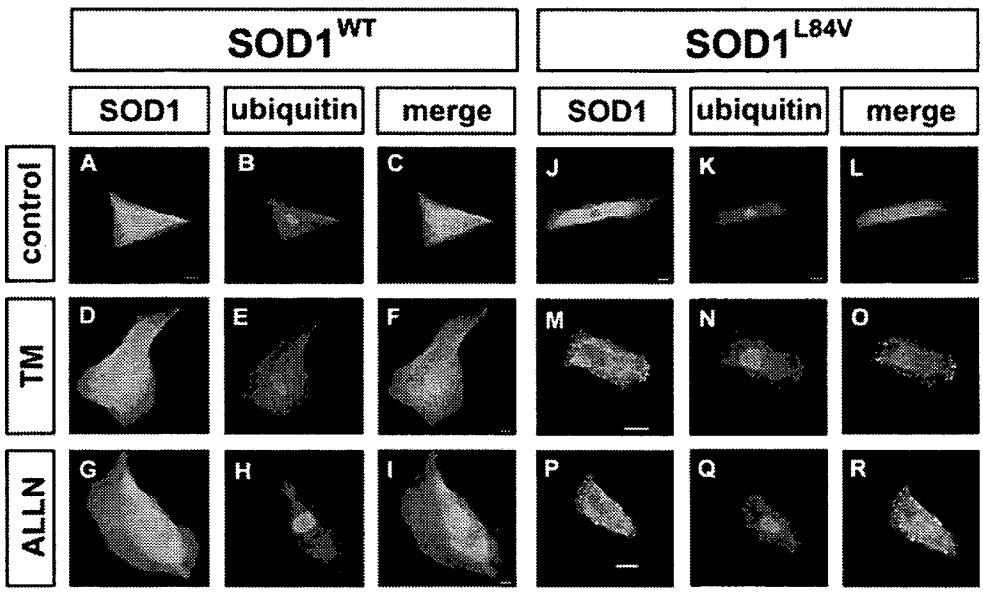

Figure 2. Ubiquitination of mutant SOD1 aggregates. (A–R) Colocalization assay with SOD1 and ubiquitin. SK-N-SH cells expressing wild-type SOD1 (A–I) or L84V SOD1 (J–R) were incubated with 1 μg/ml of tunicamycin (D–F, M–O), 4 μg/ml of ALLN (G–I, P–R), or no agents (A–C, J–L) for 24 h. Then the cells were fixed and stained with anti-SOD1 antibody (green; A, D, G, J, M, P) or anti-ubiquitin antibody (red; B, E, H, K, N, Q). Arrows indicate colocalization of SOD1 aggregates and ubiquitin. Scale bar = 20 μm. (S) Co-immunoprecipitation assay utilizing ubiquitin. SK-N-SH cells stably expressing wild-type and L84V SOD1 were transfected with a myc-tagged ubiquitin expression vector. After incubation with or without ALLN, cell lysates were prepared and assayed with anti-myc antibody of the immunoprecipitant with anti-FLAG antibody. Asterisk shows an ubiquitinated ladder that appeared after ALLN treatment of L84V SOD1-expressing cells. IgG bands are shown as loading controls.
doi:10.1371/journal.pone.0001030.g002

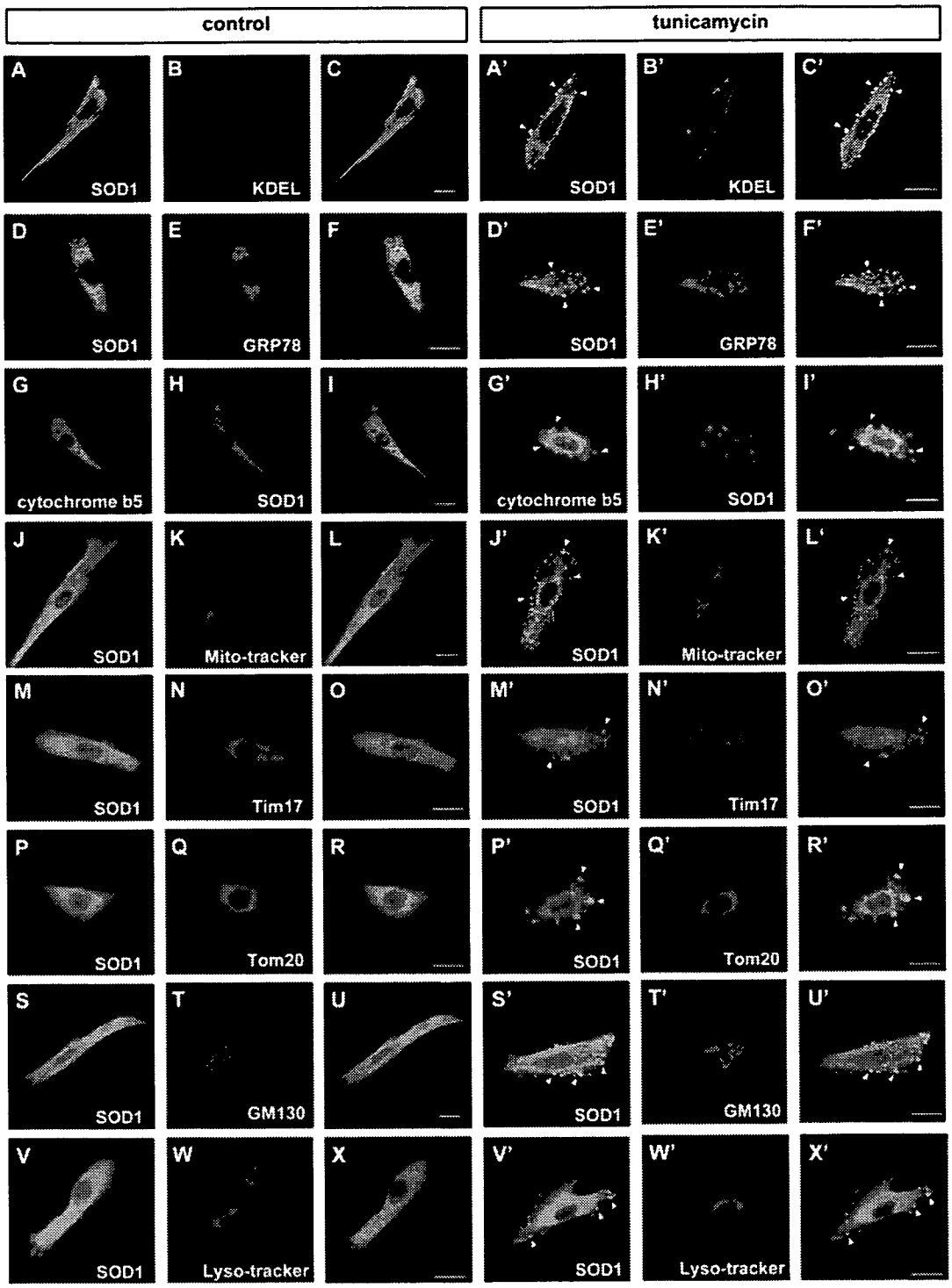

Figure 3. Positive translocation of SOD1 aggregates to ER, but not to the mitochondria, Golgi apparatus, or lysosomes. (**A–I, A'–I'**) Stress-dependent localization of SOD1 to the ER. L84V SOD1-expressing SK-N-SH cells were incubated for 24 h without (**A–I**) or with 1 μg/ml of tunicamycin (**A'–I'**). Then the cells were fixed and stained using an anti-SOD1 antibody (green; **A, D, A', D'**) and an anti-KDEL antibody (red; **B, B'**) or an anti-GRP78/BiP antibody (red; **E, E'**). GFP-cytochrome b5 were transfected to the cells and stained with anti-GFP (green; **G, G'**) and anti-SOD1 (red; **H, H'**) antibodies. Merged images (**C, F, I, C' F', I'**). The aggregates of SOD1 (arrowheads) are positive for KDEL, GRP78/BiP and cytochrome b5. (**J–R, J'–R'**) Analysis of SOD1 localization to the mitochondria. L84V SOD1-expressing SK-N-SH cells were treated as described in above. The locations of the mitochondria and SOD1 were visualized in L84V SOD1-expressing SK-N-SH cells using 100 nM Mito-tracker (red; **K, K'**), an anti-Tim17 antibody (red; **N, N'**) or an anti-Tom20 antibody (red; **Q, Q'**) and an anti-SOD1 antibody (green; **J, M, P, J', M', P'**). Merged images (**L, O, R, L', O', R'**). (**S–U, S'–U'**) Investigation of SOD1 localization to the Golgi apparatus. L84V SOD1-expressing SK-N-SH cells were treated as described in above. Then the cells were stained with anti-SOD1 antibody (green; **S, S'**) and anti-GM130 antibody (red; **T, T'**). Merged images (**U, U'**). (**V-X, V'-X'**) Analysis of the localization of SOD1 to the lysosomes. A GFP-tagged L84V SOD1 vector was transfected into L84V SOD1-expressing SK-N-SH cells. After 24 h of incubation with 1 μg/ml of tunicamycin, the cells were incubated for a further 30 min with 100 nM Lyso-tracker (red; **W, W'**) to visualize the lysosomes. GFP channel (**V, V'**) Merged images (**X, X'**). Scale bars = 20 μm. Arrowheads indicate aggregated SOD1.
doi:10.1371/journal.pone.0001030.g003

(KDEL) containing protein and GRP78/BiP, suggesting SOD1 localization in ER (Fig. 3A–F, A′–F′). In order to confirm the SOD1 colocalization with ER, we utilized GFP conjugated cytochrome b5, a typical C-terminal anchored ER membrane protein. As expected, SOD1 showed the positive staining with cytochrome b5, indicating mutant SOD1 localization to ER (Fig. 3G–I, G′–I′). In the absence of stress, ER was located to the perinuclear region. However, treatment with tunicamycin seemed to cause its relocation to an abnormal region near the cell periphery. The aberrant distribution of ER following tunicamycin treatment was not observed in cells expressing wild type SOD1 (Fig. S1C′, F′ and I′). These results suggest deterioration of ER function and localization due to aggregation of mutant SOD1.

In light of previous reports identifying mutant SOD1 colocalization to the mitochondria [34,35,37], we also examined the potential colocalization of mutant SOD1 with mitochondria. In contrast to the results with markers for ER, the SOD1 aggregates induced by tunicamycin did not colocalize with the mitochondria marker Mitotracker, with Tim17 which marks the mitochondrial inner membrane nor Tom20 which marks the mitochondrial outer membrane (Fig. 3J′–R′). The localization of these SOD1 aggregates also did not correspond with the Golgi apparatus or the lysosomes, which were stained by anti-GM130 antibody and Lyso-tracker, respectively (Fig. 3S′–X′).

Our previous results in figure 3C′, F′ and I′ revealed aberrant redistribution of ER membranes in tunicamycin-treated mutant SOD1 expressing cells to the cell periphery region. To directly visualize the localization of ER, we performed electron microscopic analysis of tunicamycin-stressed cells expressing mutant SOD1. Figure 4A and B showed abnormal aggregates of rough ER, sac-like structures with surface ribosomes, associated with numerous free ribosomes. Mutant SOD1 localization to these peripheral aggregates was confirmed by immunoelectron microscopy (Fig. 4C), implying defective functional activities of ER and free ribosomes in cells expressing mutant SOD1.

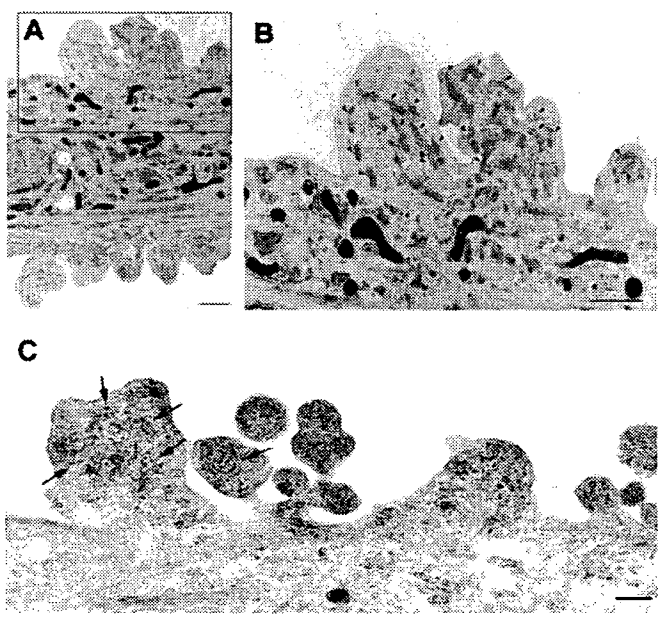

Figure 4. ER and SOD1 co-localization in peri-cytoplasmic membrane region. (A) Electron micrograph of L84V SOD1-expressing SK-N-SH cells after treatment with 1 μg/ml of tunicamycin for 24 h as described in Materials and Methods. (B) Enlargement of part of (A). Arrowheads indicate abnormal ER aggregates, where mutant SOD1 is localized as in Fig. 3C′ and 3E′. Scale bar = 1 μm. (C) SOD1 localization in peri-cytoplasmic membrane region. Cells were treated as described in (A) and immune electron micrograph was obtained as described in Materials and Methods. Arrows show SOD1 immunoreactive in ER.
doi:10.1371/journal.pone.0001030.g004

LBHI/Ast-HI-like Inclusions are induced by ER stress.

Wate et al. [28] reported that neuronal LBHI in G93A SOD1 transgenic mice are immune reactive for GRP78/BiP, an ER resident component of the UPR response. As shown in figures 3A′-I′ and 4C, mutant SOD1 localized to the ER following stress induction by tunicamycin. These SOD1 aggregates shared additional features with LBHI/Ast-HI, namely eosin positivity and ubiquitin immune reactivity. Those observations led us to consider whether ER stress would eventually induce the formation of full-fledged LBHI/Ast-HI. To test this hypothesis, we examined whether inclusion bodies containing mutant SOD1 developed in L84V SOD1-expressing cells subjected to ER stress. Consistent with this idea, eosinophilic hyaline inclusions (~10 to 20 μm in diameter) with a pale core, which are similar to neuronal LBHI/Ast-HI in the spinal cord of ALS patients harboring a SOD1 mutation, developed within 24 hrs of exposure to tunicamycin (Fig. 5A), but not in cells expressing wild type SOD1 (data not shown). In fact, the eosin-positive LBHI/Ast-HI-like hyaline inclusions (LHIs) were morphologically similar to the Ast-HI seen in the spinal cord of transgenic L84V SOD1 mice at the symptomatic stage (Fig. 5A and D). Furthermore, ultrastructual analysis revealed that the LHIs in neuroblastoma cells were composed of granule-coated fibrils (approximately 15–25 nm in diameter) and granular materials, which are the typical morpho-

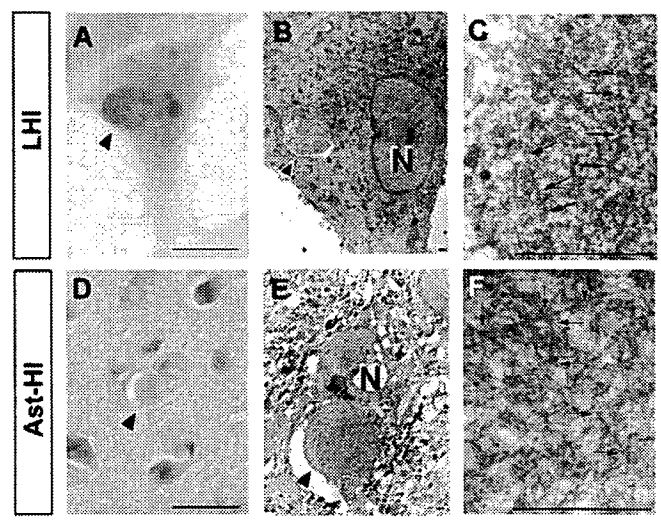

Figure 5. LHIs containing granule-coated fibrils are morphologically identical with Ast-HI from L84V transgenic mice. (A–F) Comparison of a LHI induced by ER stress in an L84V SOD1-expressing SK-N-SH cell (A–C) and Ast-HI in the spinal cord of a transgenic L84V SOD1 mouse (D–F). (A) An eosinophilic LHI in the cytoplasm of the SK-N-SH cell expressing L84V SOD1 cell was induced by treatment with 1 μg/ml of tunicamycin for 24 h (scale bar = 20 μm). (B) Electron micrograph of a hyaline inclusion (arrow) obtained by the direct epoxy resin-embedding method after decolorization of the HE-stained section shown in (A). N, nucleus; ×3000 (scale bar = 1 μm). (C) At a high magnification, the inclusion is composed of granule-coated fibrils (arrows) approximately 15–25 nm in diameter and granular materials. ×16000 (scale bar = 1 μm). (D) An eosinophilic Ast-HI from a transgenic L84V SOD1 mouse. (E) Electron micrograph of an Ast-HI obtained by the direct epoxy resin-embedding method mentioned in (B). N, nucleus; ×2000 (scale bar = 1 μm). (F) Enlargement of (E). ×16000 (scale bar = 1 μm). Note that the fibrils observed in (C) and (F) are ultrastructually identical.
doi:10.1371/journal.pone.0001030.g005

logical hallmarks of mutant SOD1-linked FALS, and were identical with the Ast-HI found in L84V SOD1 mice (Fig. 5C, F; [38]). These results suggest that LBHI/Ast-HI in FALS patients might be provoked by ER stress as we observed for LHIs.

We further explored the molecular similarity between the LHI and LBHI/Ast-HI, using double-label immunocytochemistry. As shown in figure 6A–D, LHIs induced by tunicamycin are immunopositive for anti-SOD1 and anti-ubiquitin antibodies, consistent with the LBHI/Ast-HI features. In the spinal cord of G93A SOD1 mutant mice at the symptomatic stage, neuronal LBHI show GRP78/BiP immunoreactive, suggesting the involvement of ER resident protein [28]. Therefore, we examined whether LHIs also contain ER resident protein. As expected, LHI showed anti-KDEL positivity, indicating the involvement of ER resident proteins such as calreticulin, GRP 94, PDI and GRP78/BiP in LHI development (Fig. 6E and F). Furthermore, Ast-HI in spinal cord of L84V SOD1 transgenic mice at symptomatic stage also showed KDEL positive (Fig. 6G and H), meaning that the principle features of these inclusions in neuroblastoma cells and the LBHI/Ast-HI of FALS patients are the same and implying LHI and LBHI/Ast-HI might develop in similar procedure.

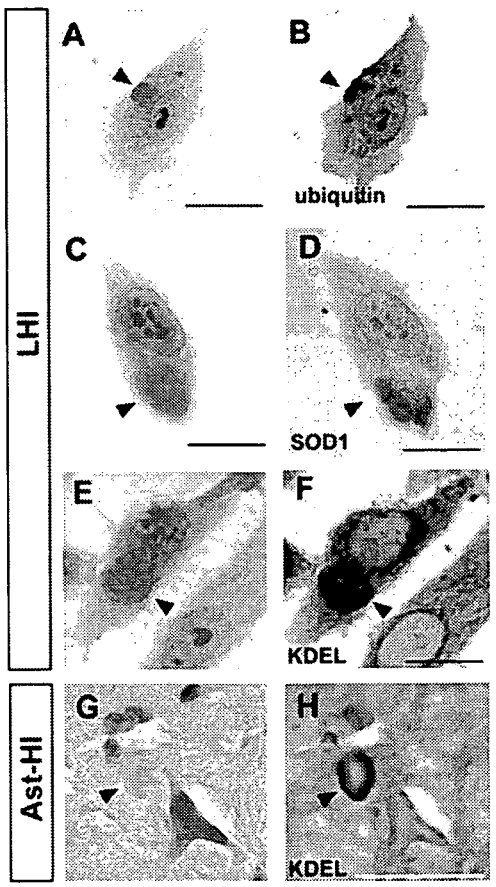

Figure 6. Positive immunoreactive against ubiquitin, SOD1 and KDEL of LHIs. (A–D) LHIs show immunoreactive against ubiquitin and SOD1. Eosinophilic LHIs in SK-N-SH cells (arrowheads in **A** and **C**) induced by tunicamycin were immunostained for ubiquitin (**B**) and SOD1 (**D**) after de-colorization. (**E–H**) KDEL immunoreactive in both LHI and Ast-HI. Eosinophilic LHI in SK-N-SH cells (arrowhead in **E**) and Ast-HI in spinal cord of L84V SOD1 mouse (arrowhead in **G**) were immunostained against anti-KDEL antibody after de-colorization (**F, H**). Scale bar = 20 μm

doi:10.1371/journal.pone.0001030.g006

Abnormal ER aggregated around peri-nuclear region with numerous free ribosomes at presymptomatic stage of Ast-HI in L84V SOD1 mice.

To further explore the relationship of LHI to the development of LBHI/Ast-HI in FALS patients with mutant SOD1, we performed ultrastructual examination of transgenic L84V SOD1 mice, which show neuronal LBHI and Ast-HI at symptomatic stage (Fig. 5D–F, 6G–H; [35]). We examined the mice at the presymptomatic stage in the hope of detecting precursors to hyaline inclusion bodies. In spinal cord neurons of the pre-symptomatic L84V SOD1 transgenic mice, we observed aberrant aggregation of electron-dense rough ER around the peri-nuclear region with numerous free ribosomes, which were suspected to be producing mutant SOD1 (Fig. 7). This suggests that the aberrant SOD1 fibrils observed in spinal neurons of these mice at later

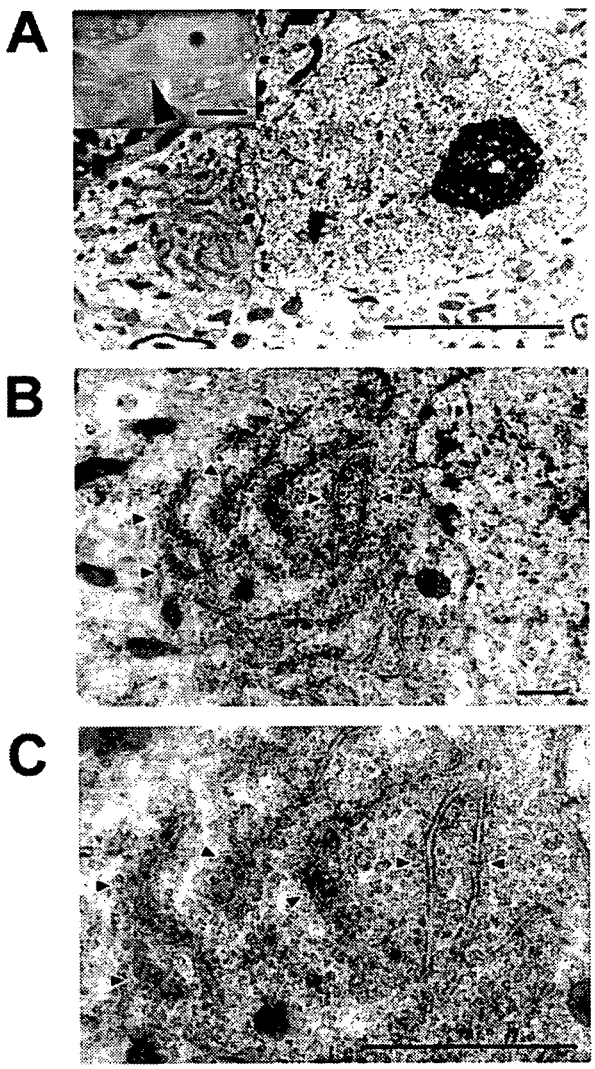

Figure 7. ER shows abnormal aggregation with numerous free ribosomes in L84V SOD1 mouse at presymptomatic stage. (A–C) Electron micrographs of a neuron obtained from an L84V SOD1 transgenic mouse containing ER aggregates. The inset in (**A**) shows a cytoplasmic inclusion-like structure (arrowhead) stained with toluidine blue. (**A**) ×3500 (scale bars = 20 μm). (**B**) ×8000 (scale bar = 1 μm). (**C**) ×15000 (scale bar = 1 μm). Arrowheads indicate abnormal ER aggregates.

doi:10.1371/journal.pone.0001030.g007

stages might be produced by cooperative activity of ER and ribosomes. These inclusion-like structures with abnormal accumulation of ER seemed likely to represent a precursor to the later neuronal LBHI observed in this line. These results imply that the deterioration of ER function and the involvement of ER might be important for formation and developing neuronal LBHI/Ast-HI in mutant SOD1 harboring FALS patients.

DISCUSSION

Aggregated proteins or inclusions are a pathological hallmark and possible causative agent of several neurodegenerative disorders including ALS [39]. While LBHI/Ast-HI have been established as morphological hallmarks of mutant SOD1-linked FALS, little is known about the formation of these structures in neurons [6]. Several in vitro systems have been provided for analysis mutant SOD1 aggregation [35,36,40], however, the relationship between mutant SOD1 aggregation *in vitro* and pathological hyaline inclusions *in vivo* remains unclear. The LHI we observed in SK-N-SH cells expressing mutant SOD1 provide a direct link between *in vitro* and *in vivo* SOD1 aggregation. To our knowledge, this is the first study to show reproducible induction of LBHI/Ast-HI like structures meeting the criteria of inclusion bodies [24,26,31,38,41].

LBHIs/Ast-HIs in human FALS consist of a chaotic mixture of cytoplasmic proteins (such as SOD1, copper chaperone for SOD (CCS), peroxiredoxin 2, and glutathione peroxidase 1), cytoskeletal proteins (such as tubulin, tau protein, and phosphorylated- and nonphosphorylated neurofilament), nuclear proteins (such as neuron-specific enolase) and synaptic proteins (such as synaptophysin [24,38,41–43]). Recently, it has been published that GRP78/BiP, an ER resident chaperon protein, is also co-localized with LBHI of G93A SOD1 mice [28]. GRP78/BiP is molecular chaperone protein induced by IRE1 in response to aberrant protein folding and promotes proper protein folding. In this context, GRP78/BiP may be acting as part of the UPR response to resolve granule coated fibrils. Tobisawa et al. [35] reported increased protein levels of GRP78/BiP in motor neurons of mutant SOD1 transgenic mice, suggesting that the motor neurons in their model suffer from 'ER stress'. While the importance of ER stress or proteosome malfunction in formation of mutant SOD1 aggregates has been established [35,36,40], the mechanisms by which mutant SOD1 forms LBHI/Ast-HI in FALS remain poorly understood. In this study, we present three lines of evidence for the involvement of ER stress in early events in LBHI/Ast-HI formation. First, ER stress in neuroblastoma cells expressing mutant SOD1 results in SOD1- and ubiquitin-immunopositive LHIs, compatible with LBHI/Ast-HI, composed of granule-coated fibrils approximately 15–25 nm in diameter and granular materials (Figs. 5 and 6). Secondly, we observed similar structures in the spinal cord of L84V SOD1 transgenic mice at pre-symptomatic stages, including abnormal electron dense, i.e. stressed, ER and numerous free ribosomes. (Figs. 4 and 7). Third, positive staining against anti-KDEL antibody, which recognizes ER resident proteins such as calreticulin, GRP 94, PDI and GRP78/BiP, were observed in both the LHI and Ast-HI of L84V SOD1 transgenic mice at symptomatic stages (Fig. 6E–H). These findings support the hypothesis that ER stress induces LBHIs/Ast-HIs creation in FALS patients with mutant SOD1. Taken together, these observations suggest that LHI in neuroblastoma cells and LBHI/Ast-HI in FALS patients might develop through similar processes.

In this study, we presented evidences that ER stress causes aggregates of mutant SOD1 and formation of LHI which is compatible with LBHI/Ast-HI. However, other questions arise from these results. 1) Why did same stress induce the different outcome of mutant SOD1 aggregation in the neuroblastoma? 2) Are the smaller aggregates competent to develop to LHIs? To answer these questions, we sought without success to identify the origin of the granule coated fibrils or SOD1 containing filamentous structure (e.g. less densely coated fibrils) in the smaller SOD1 aggregates localized to ER in L84V SOD1 expressing cells. Nevertheless, we found common features between the small aggregates in L84V SOD1 expressing SK-N-SH cells and neuronal LBHI-precursor in L84V transgenic mice, including regions of abnormal ER aggregation surrounded by abundant free ribosomes (Fig. 4B and Fig 7C). Furthermore, LHI and Ast-HI were immunopositive for the KDEL peptide present in ER-resident proteins, suggesting the involvement of ER itself in formation or development of LBHI/Ast-HI (Fig. 6E–H). We suggest that aberrant SOD1 fibril might be produced by cooperative activity of ER and ribosomes. To answer the questions, careful observation of LHI with time lapse analysis is needed.

It remains unclear why the major symptoms of ALS in patients with mutant SOD1-linked FALS do not develop until middle age, but we speculate that age-dependent changes in responses to ER stress might provide an answer. Under normal conditions, newly synthesized and misfolded proteins are refolded by chaperons such as GRP78, 94, calnexin, and calreticulin. This UPR response may be more robust in younger FALS patients and might be the reason the proteins aggregates are not observed in young patients even though mutant SOD1 is expressed. However, a decrease in protein folding or chaperone capability may occur with aging, and accumulation of misfolded proteins in the ER lumen may gradually lead to ER stress [44]. Consistent with this idea, Tobisawa et al. reported mutant SOD1 retention in the ER in COS7 cells [35] and Kikuchi et al. reported age-dependent increase of mutant SOD1 aggregation to ER in spinal cord of G93A SOD1 mice, suggesting ER dysfunction might be caused by mutant SOD1 [36]. Prolonged ER stress associated with insufficient degradation of misfolded proteins would subsequently activate apoptotic pathways. Nakagawa et al. reported that caspase-12, the ER resident caspase, is specifically cleaved and activated by ER stress, and that cells derived from mice lacking caspase-12 are resistant to ER stress [16]. In the spinal cords of G93A SOD1 mice, caspase-12 is activated in symptomatic period and can be inhibited by overexpression of XIAP (X-linked inhibitor of apoptosis protein [45,46]. Then, we analyzed activation of caspase-4 (the human orthologue of rodent caspase-12) following tunicamycin treatment. As expected, the SOD1 aggregates of the L84V SOD1-expressing neuroblastoma cells colocalized with caspase-4 (unpublished data), implying caspase-4 might contribute to cell death in our model system.

Although it can take longer than 30 years for LBHI/Ast-HI to develop in FALS patients, we could induce the formation of morphologically similar LHI within 24 hours in our simple model. Detection of the molecular targets for ER stress-induced hyaline inclusions of mutant SOD1 in our model might lead to the development of therapy that can prevent the progression of mutant SOD1-linked FALS. Ultimately, our study should contribute to the development of a simple system to analyze novel therapies for ALS.

MATERIALS AND METHODS

Transgenic Mice

Transgenic mice for mutant human SOD1^{L84V} (C587BL/6 background) were created (M. Kato, et al. Transgenic mice with ALS-linked SOD1 mutant L84V. Abstract of the 31st Annual Meeting of Society for Neuroscience, San Diego, 2001). Mice were genotyped by PCR to detect the mutant SOD1 transgene using